www.nature.com/cdd

CDDpress

ARTICLE

Ca^{2+}-mediated mitochondrial inner membrane permeabilization induces cell death independently of Bax and Bak

Giovanni Quarato[1✉], Fabien Llambi[1,5], Cliff S. Guy[1], Jaeki Min[2,6], Marisa Actis[2], Huan Sun[3], Shilpa Narina[4], Shondra M. Pruett-Miller[4], Junmin Peng[3], Zoran Rankovic[2] and Douglas R. Green[1✉]

The ability of mitochondria to buffer a rapid rise in cytosolic Ca^{2+} is a hallmark of proper cell homeostasis. Here, we employed m-3M3FBS, a putative phospholipase C (PLC) agonist, to explore the relationships between intracellular Ca^{2+} imbalance, mitochondrial physiology, and cell death. m-3M3FBS induced a potent dose-dependent Ca^{2+} release from the endoplasmic reticulum (ER), followed by a rise in intra-mitochondrial Ca^{2+}. When the latter exceeded the organelle buffering capacity, an abrupt mitochondrial *inner* membrane permeabilization (MIMP) occurred, releasing matrix contents into the cytosol. MIMP was followed by cell death that was independent of Bcl-2 family members and inhibitable by the intracellular Ca^{2+} chelator BAPTA-AM. Cyclosporin A (CsA), capable of blocking the mitochondrial permeability transition (MPT), completely prevented cell death induced by m-3M3FBS. However, CsA acted upstream of mitochondria by preventing Ca^{2+} release from ER stores. Therefore, loss of Ca^{2+} intracellular balance and mitochondrial Ca^{2+} overload followed by MIMP induced a cell death process that is distinct from Bcl-2 family-regulated mitochondrial outer membrane permeabilization (MOMP). Further, the inhibition of cell death by CsA or its analogues can be independent of effects on the MPT.

Cell Death & Differentiation (2022) 29:1318–1334; https://doi.org/10.1038/s41418-022-01025-9

INTRODUCTION

Mitochondrial outer membrane permeabilization (MOMP) is a key step in the mitochondrial pathway of apoptosis [1], arguably the most common mechanism of regulated cell death in animals [2]. MOMP is controlled by the Bcl-2 family of proteins and requires at least one of the pro-apoptotic Bcl-2 effector proteins: Bax, Bak, and Bok [3]. The anti-apoptotic Bcl-2 proteins, including Bcl-2, Bcl-xL, Mcl-1, and others, function by inhibiting Bax- or Bak-mediated MOMP [3]. Upon MOMP, the proteins of the mitochondrial intermembrane space (IMS) are released into the cytosol, and among these, cytochrome c (CytC) is responsible for activating caspases [4]. Upon CytC release, mitochondrial respiration declines, but it can be sustained if sufficient CytC is present to promote electron transfer [5]. This suggests that upon MOMP most mitochondria maintain inner mitochondrial membrane (IMM) integrity, although some mitochondria can release matrix components as well, including mitochondrial DNA [6, 7].

An alternative mechanism to induce permeabilization of the outer mitochondrial membrane (OMM) is the mitochondrial permeability transition (MPT), mediated by the opening of an incompletely defined permeability transition pore (PTP) with a suggested cutoff of about 1.5 KDa [8]. MPT is best observed in isolated mitochondria exposed to high levels of Ca^{2+} [8–11] and it results in dissipation of the mitochondrial transmembrane potential, solute diffusion, mitochondrial matrix swelling, and often physical disruption of the OMM by the expanding IMM [12]. MPT is inhibited by Cyclosporine A (CsA) and analogues that do not inhibit calcineurin [13–16]. The matrix protein Cyclophilin D (CypD) is one target of CsA [17] and regulates MPT, although at higher Ca^{2+} levels MPT proceeds in the absence of this protein [18]. Roles for the Bcl-2 proteins in regulating MPT have been proposed [19, 20] in an effort to unify the mechanisms of mitochondrial apoptosis; however, most studies of CypD and MPT appear to implicate this mechanism in necrotic cell death during ischemia-reperfusion injury, rather than apoptosis [21, 22].

2,4,6-trimethyl-N-(*m*-3-trifluoromethylphenyl) benzenesulfonamide (m-3M3FBS) is a compound originally identified as a PLC activator, leading to the inositol-3-phosphate generation and cytosolic Ca^{2+} increase [23], and it potently induces apoptosis in different cell lines [24, 25]. Therefore, we speculated that m-3M3FBS would provide a means to interrogate the relationships between mitochondrial Ca^{2+} overload and apoptosis.

[1]Department of Immunology, St. Jude Children's Research Hospital, Memphis, TN 38105, USA. [2]Department of Chemical Biology & Therapeutic, St. Jude Children's Research Hospital, Memphis, TN 38105, USA. [3]Department of Structural Biology, Department of Developmental Neurobiology, Center for Proteomics and Metabolomics, St. Jude Children's Research Hospital, Memphis, TN 38105, USA. [4]Department of Cell and Molecular Biology and The Center for Advanced Genome Engineering, St. Jude Children's Research Hospital, Memphis, TN 38105, USA. [5]Present address: Relay Therapeutics, Cambridge, MA 02139, USA. [6]Present address: Amgen Inc., Thousand Oaks, CA 91320, USA.
✉email: giovanni.quarato@stjude.org; douglas.green@stjude.org

Edited by G. Melino

Received: 11 November 2021 Revised: 27 May 2022 Accepted: 3 June 2022
Published online: 20 June 2022

We found that treatment of cells with m-3M3FBS caused a rapid Ca^{2+} efflux from the ER to the cytosol and Ca^{2+} uptake into the mitochondrial matrices. This was followed by Ca^{2+}-dependent, mitochondrial *inner* membrane permeabilization (MIMP) and then by a slow IMS protein release, indicative of OMM rupture. This contrasted with the kinetics of Bax- and Bak-mediated MOMP, which allowed rapid release of IMS proteins with almost undetectable release of matrix proteins. Unlike MOMP, m-3M3FBS-induced MIMP was independent of Bax and Bak and was not inhibited by anti-apoptotic proteins. CsA and analogues capable of blocking MPT completely prevented cell death induced by m-3M3FBS. CsA acted upstream of mitochondria to prevent Ca^{2+} release from ER stores. Among several well-known Ca^{2+} agonists, we also identified Arachidonate as an inducer of MIMP. Our results suggest that mitochondrial Ca^{2+} overload triggers a cell death process distinct from Bcl-2 family-regulated MOMP, and further, that the inhibition of cell death by CsA or its analogues can be independent of its effects on the MPT.

RESULTS

m-3M3FBS induces ER to cytosol and mitochondrial matrix Ca^{2+} redistribution followed by mitochondrial depolarization

We employed the putative PLC agonist m-3M3FBS to induce a generalized intracellular calcium mobilization, as shown by cytosolic Ca^{2+} spikes, detected by Oregon Green™ 488 BAPTA-1 AM in fast fluorescence lifetime imaging microscopy (FLIM) (Fig. 1a) [26]. A per-cell based analysis showed cytosolic Ca^{2+} spikes in the range of 25–200 nM (Fig. 1b). Notably, increasing m-3M3FBS concentration accelerated the onset but not the amplitude of the Ca^{2+} spike (Fig. S1a).

To examine Ca^{2+} levels in specific cellular compartments, we took advantage of the green calcium sensor GCaMP3 [27] targeted to the mitochondrial matrix. Upon m-3M3FBS treatment we observed a rapid (approx. 200–400 s) increase in mitochondrial Ca^{2+} in a variety of cell lines (Fig. 1c, Supplementary Movies 1–3). We then combined the use of GCaMP3 and another red calcium sensor, GECO [28], to simultaneously visualize Ca^{2+} in different cellular compartments, targeting the sensors to the mitochondrial matrix, cytosol, and endoplasmic reticulum (ER) lumen. Treatment with m-3M3FBS caused a rapid release of Ca^{2+} from the ER and a rise in cytosolic Ca^{2+} (Fig. 1d top, Supplementary Movie 4). This Ca^{2+} efflux from the ER to the cytosol was accompanied by an uptake of Ca^{2+} into the mitochondria (Fig. 1d, center and bottom, Supplementary Movies 5, 6), quickly followed by mitochondrial Ca^{2+} release and depolarization (Fig. 1e). m-3M3FBS treatment triggered a prompt and complete loss of oxygen coupled respiration (OCR), accompanied by a transitory increase in glycolysis (ECAR, Fig. 1f). Therefore, m-3M3FBS induces a sudden Ca^{2+} release from the ER, initially buffered by mitochondria, that eventually leads to mitochondrial calcium overload and respiratory failure.

m-3M3FBS induces mitochondrial calcium overload, inner mitochondrial membrane permeabilization and cell death independently of necroptosis and pyroptosis

To determine the consequences of a rapid mitochondrial Ca^{2+} increase, we employed super-resolution (SIM) microscopy of cells expressing the mitochondrial matrix protein TFAM fused to mCherry. After 3 min of treatment with m-3M3FBS, we observed the release of mCherry from mitochondria and into the cytosol (Fig. 2a). A mitochondrial permeabilization assay similarly showed that the mitochondrial matrix proteins Mn-Superoxide Dismutase (MnSOD) and CypD were released upon treatment with m-3M3FBS (Fig. 2b). In contrast, after a pretreatment with a sublethal dose of UV irradiation to synchronize the onset of MOMP [29], only a minor MnSOD and CypD release was observed upon treatment with MOMP-inducing BH3-mimetic drugs (Fig. 2b), likely as a consequence of matrix herniation [6, 7]. Therefore, m-3M3FBS induces rapid mitochondrial inner membrane permeabilization (MIMP).

Transmission electron microscopy revealed that within 15 minutes of treatment with m-3M3FBS, mitochondria appeared swollen with a loss of cristae structure (Fig. 2c, green arrows) as well as enlargement of mitochondria associated ER lumen (pink arrows). When we examined the kinetics of cell death, the increase in mitochondrial Ca^{2+} was again observed within 2–4 min of m-3M3FBS treatment (Fig. S2a), with the earliest evidence of cell death (loss of plasma membrane integrity) beginning in about 30 minutes and continuing over several hours (Fig. 2d, e). The inactive isomer, o-3M3FBS, did not induce cell death (Fig. S2b).

While m-3M3FBS is described as a Phospholipase c (PLC) activator, it was effective in inducing cell death in cells lacking PLCγ1 or PLCγ2 (Fig. S2c) (Tables S1, S2) or in the presence of the PLC inhibitor U73122 (Fig. S2d), as previously reported [30].

The Gasdermins are pore forming proteins that mediate pyroptotic/secondary necrotic cell death through membrane rupture [31–33]. m-3M3FBS treatment resulted in a pyroptosis-like cell death morphology (Fig. 2e) and induces pyroptosis in macrophages [34]. To determine if Gasdermins regulate m-3M3FBS-induced cell death, we silenced each of them (Fig. S2e). In no case did such silencing affect the extent of m-3M3FBS cytotoxicity (Fig. S2f). Similarly, m-3M3BFS also induced cell death in the absence of the necroptosis effectors Receptor Interacting Protein Kinase 3 (RIPK3) or Mixed Lineage Kinase Like (MLKL) [35–37] (Fig. S2g, h). Therefore, m-3M3FBS-induced cell death is independent of both the pyroptotic and necroptotic machinery in HeLa cells and MEFs.

MIMP is kinetically distinct from MOMP and is not regulated by the Bcl-2 family proteins

To compare the kinetics of MIMP and MOMP, we co-expressed mitochondrial matrix-targeted GCaMP3 (mito-GCaMP3) and the IMS protein Omi tagged with mCherry (Omi-mCherry) in HeLa cells and examined their release upon MOMP (treatment with BH3-mimetics) and MIMP (treatment with m-3M3FBS). To synchronize the onset of MOMP, cells were primed with a sublethal dose of UV irradiation [29]. Induction of MOMP with a Bcl-2 and Bcl-xL inhibitor ABT-737 triggered a sudden release of Omi-mCherry with little or no release of mito-GCaMP3 (Fig. 3a, b, left panels, Supplementary Movie 7). In contrast, m-3M3FBS induced a rapid increase in mito-GCaMP3 fluorescence (corresponding to the calcium spike), followed by its sudden and rapid release from the mitochondria (Fig. 3a, b, right panels, Supplementary Movie 8). In contrast to MOMP, Omi-mCherry release from the IMS following MIMP was slower than the release observed in cells undergoing MOMP (Fig. 3b).

The Bcl-2 effector proteins, Bax, Bak, and Bok are required for MOMP during apoptosis [3]. Anti-apoptotic Bcl-2 proteins inhibit this function of Bax and Bak [38], and Bok is regulated by ER-associated degradation [39]. HeLa cells lacking both Bax and Bak (Fig. S3a) were completely resistant to cell death induced by BH3-mimetics but fully susceptible to cell death induced by m-3M3FBS (Fig. 3c). During apoptosis, MOMP releases CytC to activate APAF1 and caspases [40]. Silencing of APAF1 (Fig. S3b) delayed cell death in both settings (Fig. 3d), suggesting that both MOMP and MIMP can engage caspase activation to facilitate cell death.

We then over-expressed the anti-apoptotic Bcl-2 proteins Bcl-2, Bcl-xL, and Mcl-1 (Fig. S3c) to evaluate their ability to reduce steady-state $[Ca^{2+}]_{er}$ and mitochondrial Ca^{2+} uptake [41, 42]. Their expression rendered cells resistant to apoptosis induced by Actinomycin D or Staurosporine and displayed sensitivity to the appropriate BH3-mimetic drug (ABT-737 for Bcl-2 and Bcl-xL, S63845 for Mcl-1, or their combination) (Fig. S3d). Interestingly, HeLa overexpressing Bcl-xL and Mcl-1 showed a reduced intensity of Ca^{2+} spikes after treatment with m-3M3FBS (Fig. 3e);

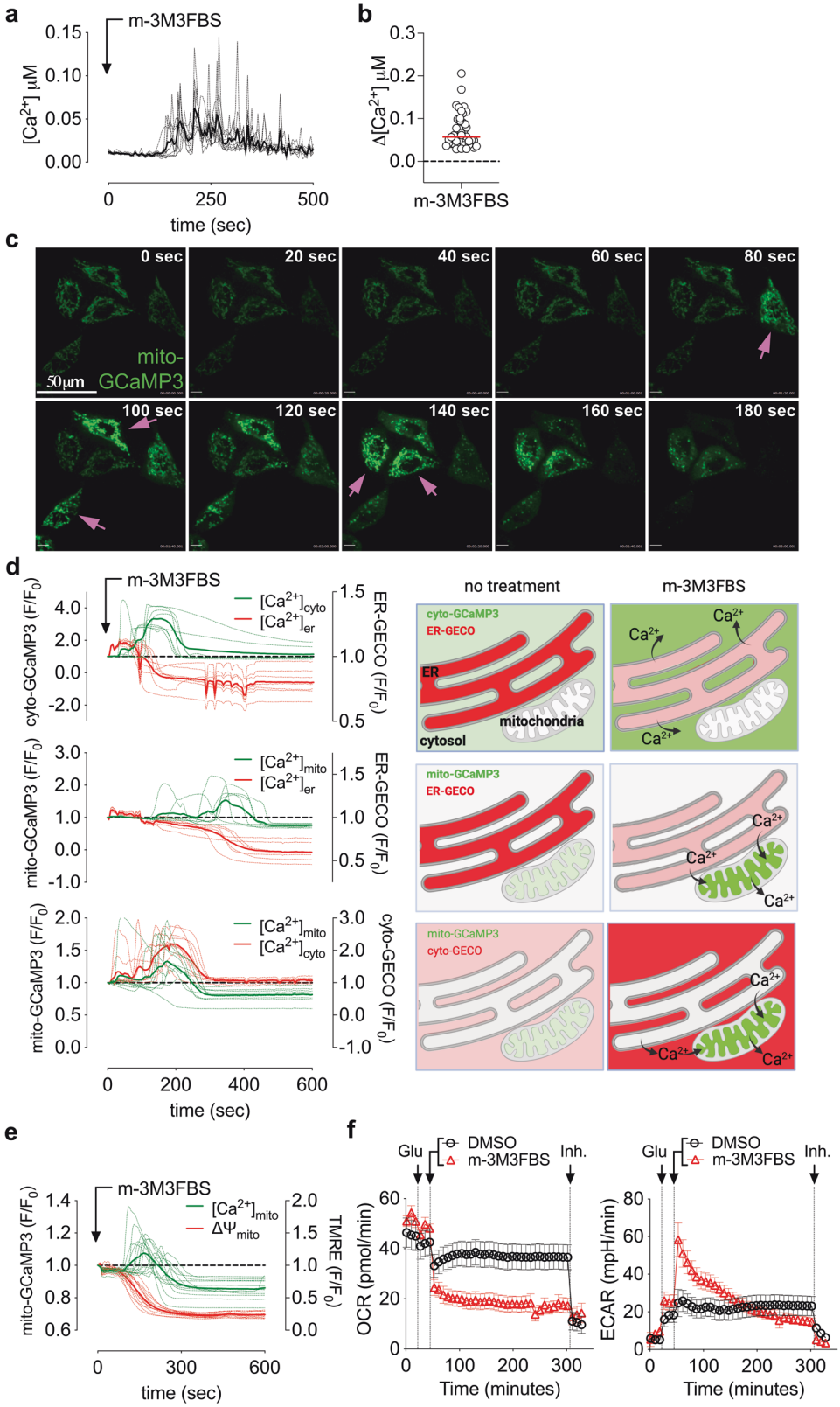

nevertheless, expression of the anti-apoptotic Bcl-2 proteins had no effect on the mitochondrial Ca^{2+} uptake, MIMP (Fig. S3e, f) and kinetic or extent of cell death induced by m-3M3FBS (Fig. 3f). In summary MIMP, differently from MOMP, is not regulated by Bcl-2 family proteins.

Intracellular Ca^{2+} chelation blocks m-3M3FBS-induced cell death

Several ionic channel families regulate intracellular Ca^{2+} trafficking (Fig. S4a). We speculated that their pharmacological manipulation could resemble m-3M3FBS effects. We therefore tested Thapsigargin,

Fig. 1 m-3M3FBS induces intracellular calcium mobilization and mitochondrial calcium overload. a FLIM intracellular calcium quantification in HeLa cells after treatment with 25 μM m-3M3FBS. Each dashed line represents one single cell in the field. The continuous bold line represents the mean signal from all the cells in the field. Cells were pre-labeled with 4 μM of Oregon Green™ 488 BAPTA-1, AM. Data are representative of $n = 4$ independent experiments. **b** Intracellular Ca^{2+} spike quantification using FLIM. Each dot represents the highest $\Delta[Ca^{2+}]$ value recorded for each cell. $\Delta[Ca^{2+}]$ was calculated as maximum amplitude of $[Ca^{2+}]$ oscillation from $[Ca^{2+}]_{t=0}$. Cells were pre-labeled with 4 μM of Oregon Green™ 488 BAPTA-1, AM. Data are from $n = 4$ independent experiments. **c** Confocal microscopy analysis showing matrix mitochondrial calcium accumulation using mito-GCaMP3 in HeLa cells after treatment with 25 μM m-3M3FBS; magenta arrows indicate cells undergoing transitory mitochondrial matrix calcium accumulation. Data are representative of $n = 3$ independent experiments. Scale bar = 50 μm. **d** Intracellular calcium mobilization in HeLa cells after treatment with 25 μM m-3M3FBS (as fluorescence F/F_0 arbitrary units) with a schematic representation of the results. Upper panel: cytosolic calcium (cyto-GCaMP3) vs ER lumen calcium (ER-GECO). Middle panel: mitochondrial matrix calcium (mito-GCaMP3) vs ER lumen calcium (ER-GECO). Lower panel: matrix mitochondrial calcium (mito-GCaMP3) vs cytosolic calcium (cyto-GECO). Each dashed line represents one single cell in the field. The continuous bold line represents the mean signal from all the cells in the field. Data are representative of $n = 4$ independent experiments. **e** Matrix mitochondrial calcium accumulation using mito-GCaMP3 and mitochondrial transmembrane potential in HeLa cells after treatment with 25 μM m-3M3FBS; 200 nM TMRE was preincubated 5′ before beginning of the experiment. Data are representative of $n = 3$ independent experiments. **f** OCR and ECAR of HeLa cells treated as indicated by the arrows using a Seahorse XFe bioanalyzer. "Glu" = 10 mM glucose and "Inh." (inhibitors) = 0.5 μM rotenone + 0.5 μM antimycin A (for OCR) and 50 mM 2-deoxy-glucose (for ECAR), as detailed in Methods section. m-3M3FBS was used at 25 μM. Error bars represent the SEM from the mean of $n \geq 13$ samples. Data are representative of $n = 3$ independent experiments.

which blocks ER Ca^{2+} uptake by SERCA, increasing Ca^{2+} release from ER calcium stores [43, 44]. Like m-3M3FBS, Thapsigargin induced intracellular Ca^{2+} mobilization (Fig. S4b), albeit with a significantly lower range of Ca^{2+} spikes (Fig. 4a). Interestingly, when compared to m-3M3FBS, Thapsigargin showed a delayed mitochondrial Ca^{2+} uptake that was not followed by MIMP (Fig. 4b), suggesting that the route, intensity, and frequency in Ca^{2+} spikes regulate MIMP and cell death.

To assess whether m-3M3FBS-induced cell death was due to a calcium overload, we employed the intracellular Ca^{2+}-chelator BAPTA-AM. Pre-incubation with this chelator completely blocked m-3M3FBS-induced cell death (Fig. 4c), while we found no effect of chelating extracellular Ca^{2+} with EGTA (Fig. S4c), confirming that Ca^{2+} originated in ER stores. The Ca^{2+}-buffering protein parvalbumin (PVALB) was recently reported to regulate cell growth, proliferation, and death [45–47]. To test its ability to chelate Ca^{2+} in our setting, we expressed in HeLa cells a cytosol- and a mitochondria-targeted form of the protein (Fig. S4d, e), but no significant change in MIMP or cell death was observed after m-3M3FBS treatment (Fig. 4d, e).

Other Ca^{2+} mobilization inducers are associated with cell death [44]. Arachidonate and C_2-ceramide (C_2-cer.), both lipid mediators, initiate apoptosis after Ca^{2+} release from ER and MPT [44, 48–50], similar to H_2O_2, the oxidant stressor prototype [51]. To examine their ability to induce MIMP rather than MOMP, we examined in HeLa cells the release of a mitochondrial matrix-targeted Cerulean protein ($COX8A_{1-29}$-Cerulean) and the IMS protein Omi-mCherry. Among them, Arachidonate-induced MIMP (Fig. 4f) and cell death in a Bax, Bak-independent manner in media with 2% FBS (Fig. 4g). FBS absorbs Arachidonate, a lipophilic compound, decreasing its bio-availability 50–100 times when compared with the input concentration [52]. The use of media containing 10% FBS abolished Arachidonate-induced MIMP and promoted MOMP (Fig. 4h), observed as Bax,Bak-dependent cell death (Fig. 4i). Increasing Arachidonate concentrations accelerated intracellular Ca^{2+} spike onset and amplitude (Fig. S4f). Finally, both Thapsigargin and C_2-cer. induced apoptosis [44, 53], while H_2O_2 showed a necrotic-type of Bax,Bak-independent cell death [54, 55] (Fig. 4i).

Taken together, our results suggested that intracellular Ca^{2+} chelation protected from m-3M3FBS cytotoxicity. Moreover, Arachidonate triggered MIMP and Bax,Bak-independent cell death.

m-3M3FBS-dependent MIMP and cell death does not rely on the main ER-mitochondria Ca^{2+} route

To identify potential mechanisms of Ca^{2+} release from ER affecting cell death, we used Xestospongin C (IP_3 receptor, ITPR, inhibitor), and Dantrolene (ER Ryanodine receptor inhibitor). Neither of these inhibitors, alone or in combination, prevented cell death induced by m-3M3FBS (Fig. 5a).

We then ablated the three ITPR genes, obtaining a highly edited Hela ITPR triple knock-out pool cell line (sgITPR TKO) (Tables S1, S2) and tested different Ca^{2+} agonists using FLIM Ca^{2+} quantification. As expected, Ca^{2+} mobilization by Histamine, a Ca^{2+} IP_3-generating agonist, was reduced in the sgITPR TKO cells (Fig. 5b) [56], unlike Thapsigargin, whose Ca^{2+} release in the cytosol was independent of ITPR activity (Fig. 5b). Notably, treatment with m-3M3FBS increased Ca^{2+} release in sgITPR TKO cells (Fig. 5b), but no differences were observed in cell death (Fig. 5c), arguing against a primary role of ITPR in this context.

MCU is the IMM calcium uniporter involved in buffering high levels of cytosolic Ca^{2+} [57–59]. Silencing of MCU or of OPA1, regulating IMM structure and protecting from Ca^{2+} overload lethality [60], had no inhibitory effect on m-3M3FBS cytotoxicity (Figs. 5d, S5a). Moreover, silencing of MCU did not affect m-3M3FBS-dependent Ca^{2+} import into mitochondria (Fig. S5b), suggesting the possible involvement of LETM1, the other known mitochondrial Ca^{2+} channel import system [61]. Nonetheless, LETM1 silencing did not show any protection from m-3M3FBS cell death (Figs. 5e, S5c). To address a possible redundancy in their function, we created a HeLa MCU,LETM1 deficient cell pool and we isolated two HeLa $MCU^{-/-}LETM1^{-/-}$ double knock-out (DKO) clones (Fig. S5d) (Tables S1, S2). Again, no protection was observed upon m-3M3FBS treatment (Fig. 5f). Moreover, the HeLa MCU,LETM1 DKO pool displayed intramitochondrial Ca^{2+} uptake and MIMP when treated with m-3M3FBS but not after Thapsigargin treatment, used as control (Fig. 5g).

A rise in cytosolic Ca^{2+} can activate calpains. However, a calpain inhibitor did not protect from m-3M3FBS cytotoxicity, while the caspase inhibitor, qVD-oph (qVD), showed a partial effect in both parental and Bax,Bak-deficient HeLa cells. As a control, qVD inhibited BH3-mimetic cytotoxicity in parental HeLa cells (Fig. 5h). During cell death, peptidases destroy intermediate filaments and promote loss of cell integrity [62, 63]. We therefore tested agents that sustain cytoskeleton polymerization. While neither jasplakinolide (actin polymerizer) nor docetaxel (microtubule polymerizer) affected cell death, the vimentin polymerizer, withaferin A, delayed cell death induced by m-3M3FBS (Fig. 5i).

Therefore m-3M3FBS-induced Ca^{2+} mobilization is largely independent of ITPRs, MCU, and LETM1, suggesting redundant mechanisms contributing to cytosolic Ca^{2+} increase and its mitochondrial uptake. Further, m-3M3FBS treatment triggered the loss of cytoskeleton integrity that is a feature of this cell death.

Cyclosporine A blocks Ca^{2+} release from ER, preventing MIMP and cell death independent of cyclophilins

An increase in Ca^{2+} in isolated mitochondria induces MPT mediated by PTP, leading to mitochondrial swelling [8]. We therefore examined the effect of CsA and the analogues, NIM-811

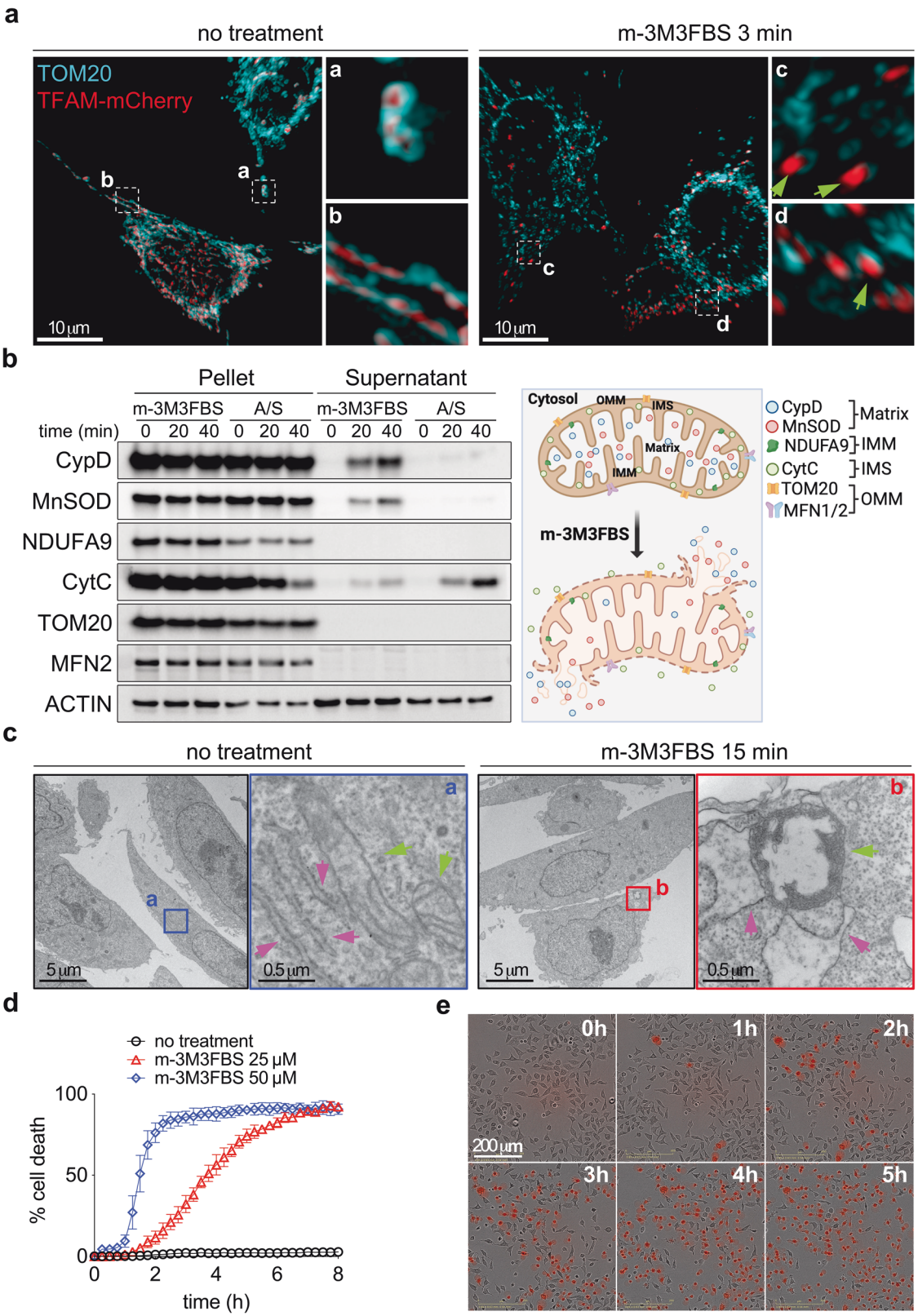

and Alisporovir, that inhibit MPT, on m-3M3FBS treatment and found that they completely blocked cell death (Figs. 6a, S6a). Further, CsA maintained clonogenic growth following m-3M3FBS treatment (Fig. 6b), while qVD, which only partially and temporarily protected against m-3M3FBS-induced cell death (Fig. 5h), did not (Fig. 6b). Even when CsA was used at saturating levels, a UPLC analysis revealed that the m-3M3FBS concentration remained relatively unchanged, ruling out a decrease in m-3M3FBS levels due to precipitation or chemical interactions between the two drugs (Fig. S6b).

Fig. 2 Mitochondrial calcium overload induces mitochondrial inner membrane permeabilization and cell death. a SIM images of HeLa cells after 3 min treatment with 25 μM m-3M3FBS: cyan: TOM20 (outer mitochondrial membrane), red: TFAM-mCherry (mitochondrial matrix); green arrows indicate release of mitochondrial matrix protein into the cytosol. Representative image of $n = 3$ independent fields per condition. Scale bar = 10 μm. **b** Immunoblot analysis showing release of soluble mitochondrial proteins into the cytosol after treatment with 25 μM m-3M3FBS or a combination of Bcl-2/Bcl-xL (5 μM ABT-737) and Mcl-1 (5 μM S63845) inhibitors for 20 and 40 min followed by digitonin permeabilization in HeLa cells. To synchronize the onset of MOMP, cells were primed with a sublethal dose of UV irradiation (5 mJ/cm^2) 16 h prior to ABT-737 plus S63845 addition. Data are representative of $n = 3$ independent experiments. **c** TEM analysis of HeLa cells after treatment with 25 μM m-3M3FBS for 15 min; green arrows indicate mitochondria, magenta arrows indicate ER. Scale bar = 5 μm. Scale bar for magnified images = 0.5 μm. **d** Kinetic analysis of cell death in HeLa cells after treatment with m-3M3FBS using an IncuCyte imaging system. Error bars represent the SD from the mean of triplicate samples. Data are representative of $n = 4$ independent experiments. **e** Representative IncuCyte images at 1 h intervals of PI-stained HeLa cells after treatment with 25 μM m-3M3FBS. Related to **d**. Scale bar = 200 μm.

The best characterized target of CsA that participates in MPT is CypD, encoded by *ppif*. However, we observed no effect of *ppif* ablation on m-3M3FBS-induced cell death in MEFs, while CsA prevented cell death in these cells (Figs. 6c, d, S6c, Supplementary Movies 9, 10).

Recently, the existence of two redundant channels, both CsA sensitive, was proposed to form the PTP: A-PTP formed by the Adenine Nucleotide Translocator family members (ANT) [64] and F-PTP derived from F-ATP synthase [65]. To address their roles, we silenced subunit g of the F-ATP synthase (Fig. S6d, e), required for F-PTP function [65], and we used bongkrekic acid to inhibit ANT [66] and therefore A-PTP [64, 65]. Neither of these treatments protected from m-3M3FBS cytotoxicity (Fig. 6e, f). Similar results were observed for other proteins previously suggested to regulate MPT-dependent cell death [67–70], namely SPG7 and VDAC family members (Figs. 6g, S6f). Nevertheless, limitations of siRNA and possible functional redundancy may explain these negative results.

To identify potential additional targets of CsA, we synthesized an analogue containing a biotin moiety and a photoactivatable diazirine group (Fig. S6g) and confirmed that it retained the ability to inhibit m-3M3FBS cytotoxicity (Fig. S6h). Using this probe, CsA-PA-Biotin, we captured proteins interacting with CsA (Fig. S6i) and identified them by mass spectrometry (Table S3). We noted several Cyclophilins associated with CsA in addition to CypD, as previously reported [71]. We then systematically silenced each of these proteins expressed in HeLa cells (Table S4, adapted from [72]; Fig. S6j), but no protection from m-3M3FBS cytotoxicity was observed (Fig. 6h). It remains possible that functional redundancy in Cyclophilins accounted for the observed lack of effect. Alternatively, we considered the possibility that CsA acts via a different mechanism to block m-3M3FBS-induced cell death.

We also identified ERK1/2 (MAPK1 and MAPK3) bound to the CsA probe. It has been reported that CsA activates ERK1/2 [73] and that ERK1/2 protects from cell death through MPT inhibition [74]. However, ERK1/2 inhibitors did not influence CsA protection from m-3M3FBS cytotoxicity (Fig. S6k).

If, indeed, CsA inhibits m-3M3FBS cytotoxicity via MPT inhibition, Ca^{2+} release from ER stores should be unaffected, as this event is upstream of the MPT. Remarkably, upon m-3M3FBS treatment, the presence of CsA or its analogue Alisporivir, prevented the rise in intracellular Ca^{2+} (Figs. 6i, S6l), the release of Ca^{2+} from ER stores and its subsequent uptake by mitochondria (Fig. 6j), suggesting that CsA regulated ER Ca^{2+} release by an additional unknown mechanisms.

High concentrations of Arachidonate, similarly to m-3M3FBS, induced MIMP and Bax,Bak-independent cell death. Notably, CsA strongly delayed cell death (Fig. 6k), supporting a common mechanism of action for those two Ca^{2+} mobilizers.

Therefore, the ability of CsA to block MIMP and cell death induced by m-3M3FBS appears to be independent of any direct effect on the PTP.

DISCUSSION

We found that upon treatment with m-3M3FBS, Ca^{2+} is released from ER stores to the cytosol and is then taken up by mitochondria, exceeding the buffering capability of the organelle. The resulting Ca^{2+} overload causes dramatic mitochondrial swelling, often suggestive of an MPT, and death of the cell, which was blocked by the Ca^{2+} chelator, BAPTA-AM. Remarkably, while CsA and analogues capable of blocking MPT in isolated mitochondria completely prevented cell death, this appeared to be due to inhibition of ER Ca^{2+} release rather than an effect on mitochondria.

We observed distinct differences between the effects of Ca^{2+} overload versus BH3-mimetic inhibition of anti-apoptotic Bcl-2 proteins on mitochondrial membrane permeabilization events. Ca^{2+} overload induced rapid and sudden release of matrix proteins (MIMP) to the cytosol with a slower, gradual release of mitochondrial IMS proteins; in contrast, BH3-mimetics induced a rapid MOMP with a minor permeabilization of the IMM. In the latter setting, the Bcl-2 effector proteins Bax and Bak were required for MOMP, but these effectors were completely dispensable for MIMP and cell death induced by Ca^{2+} overload.

A possible explanation for the slow release of IMS protein after MIMP, when compared to MOMP, lies in the cristae architecture that preserves the fast and complete release of CytC and other IMS proteins in the absence of a proper apoptotic stimulus [75, 76]. While MOMP can cause caspase-independent cell death (CICD), probably due to the catastrophic collapse of mitochondrial functions [77], such cell death is much slower than caspase-dependent apoptosis and inhibition of caspases therefore dramatically delays cell death (as measured by loss of plasma membrane integrity). In contrast, inhibition of caspase activation by silencing APAF1 in Bax,Bak-deficient cells had little effect on the kinetics of death induced by m-3M3FBS. Moreover, CICD observed after m-3M3FBS treatment is likely due to a generalized intracellular Ca^{2+} imbalance. Our EM analysis (Fig. 2c) showed several cellular organelles, such as ER, critically compromised at the structural level. Whether these changes contribute to cell death is unclear. Future studies with a "mito-depletion" system may address the central role of mitochondria and MIMP in this form of cell death [78].

The inhibition of cell death by CsA or its analogues is often taken as evidence that the cell death occurred after MPT [79, 80]. However, our finding that CsA and a CsA analogue inhibit the release of Ca^{2+} from ER stores suggests that, when such inhibition of cell death is observed, the hypothesis that the death occurs by MPT may not always be supportable. Loss of ER Ca^{2+} can result in an unfolded protein response, leading to expression and stabilization of the BH3-only protein, Bim, which activates Bax and Bak to promote MOMP and apoptosis [81]. In contrast, our results suggest that when mitochondrial Ca^{2+} overload is responsible for cell death, such cell death is independent of Bax and Bak function and is not inhibited by anti-apoptotic family members.

While CsA inhibited ER Ca^{2+} release and cell death, inhibitors of ER calcium channels and genetic manipulation of the ITPR family members did not. This suggests that other mechanisms allowed spikes of cytosolic Ca^{2+}, which presumably were sufficient for mitochondria Ca^{2+} overload and cell death to occur. Interestingly, one report concluded that CsA can inhibit

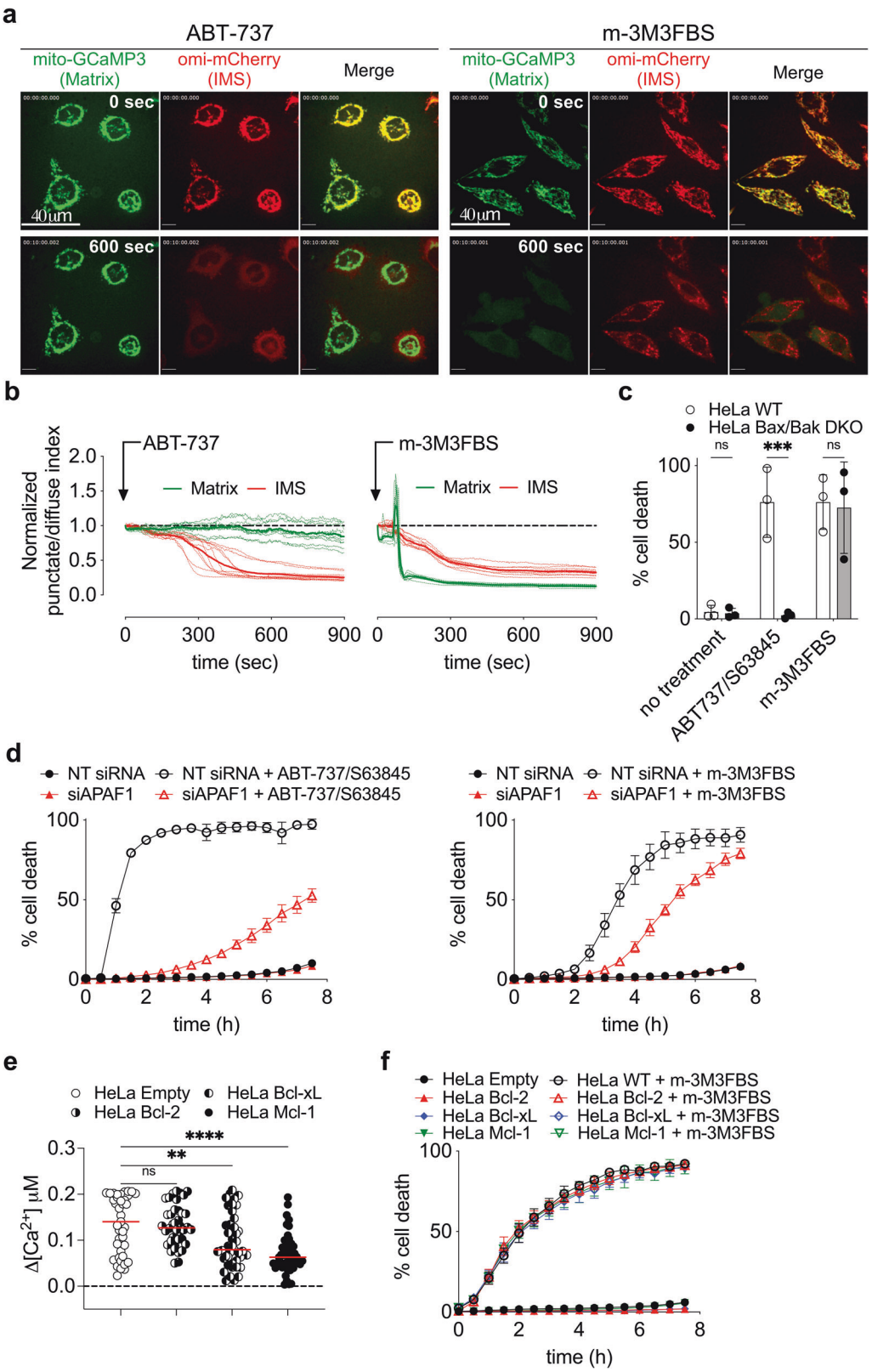

IP_3 interaction with its receptors [82], but, given our results with the sgITPR3 TKO pool, we can only suggest that CsA blocks ER Ca^{2+} release by an additional, unknown mechanism. One possibility is that m-3M3FBS alters ER permeability and that CsA preserves membrane integrity.

We employed m-3M3FBS to study the effects of elevated cytosolic Ca^{2+} on mitochondria and cell death, but such elevation can occur in response to a range of physiological and pathological situations. For example, ceramide, Arachidonate, histamine, and hydrogen peroxide induce elevated cytosolic Ca^{2+} and can induce

Fig. 3 MIMP is a kinetically distinct process than MOMP and it is not regulated by Bcl-2 family members. a Confocal microscopy analysis showing release of the IMS proteins omi-mCherry (red) and the Matrix proteins mito-GCaMP3 (green) in HeLa cells after 10 min treatment with 5 μM ABT-737 or 25 μM m-3M3FBS. To synchronize the onset of MOMP, cells were primed with a sublethal dose of UV irradiation (5 mJ/cm^2) 16 h prior to ABT-737 addition. Data are representative of $n = 3$ independent experiments. Scale bar = 40 μm. **b** Release kinetics of IMS proteins (omi-mCherry, red) and Matrix proteins (mito-GCaMP3, green) in HeLa cells after treatment with ABT-737 or m-3M3FBS. Experimental conditions are the same as in **a**. Regions were drawn around cells, and punctate/diffuse indices were plotted and displayed relative to the start of the treatment (time point 0). Each dashed line represents one single cell in the field ($n \geq 9$). The continuous bold line represents the mean signal from all the cells in the field for each marker. Data are representative of $n = 3$ independents experiments. **c** Cell death quantification of HeLa WT and Bax,Bak DKO cells after 6 h of treatment with 25 μM m-3M3FBS or 5 μM ABT-737 + 5 μM S63845 using an IncuCyte imaging system. Error bars represent the SD from the mean of $n = 3$ independent experiments. **d** Kinetic analysis of HeLa cells treated with 25 μM m-3M3FBS or 5 μM ABT-737 + 5 μM S63845 after silencing of APAF1 using an IncuCyte imaging system. Error bars represent the SD from the mean of triplicate samples. Data are representative of $n = 3$ independent experiments. **e** Intracellular Ca^{2+} spike quantification using FLIM in HeLa cells overexpressing HA-Bcl-2, HA-Bcl-xL and HA-Mcl-1 after treatment with 25 μM m-3M3FBS. Each dot represents the highest $\Delta[Ca^{2+}]$ value recorded per cell. $\Delta[Ca^{2+}]$ was calculated as maximum amplitude of $[Ca^{2+}]$ oscillation from $[Ca^{2+}]_{t=0}$. Cells were pre-labeled with 4 μM of Oregon Green™ 488 BAPTA-1, AM. Data are from $n = 4$ independent experiments. **f** Kinetic analysis of cell death in HeLa cells overexpressing HA-Bcl-2, HA-Bcl-xL and HA-Mcl-1 after treatment with 25 μM m-3M3FBS. Error bars represent the SD from the mean of triplicate samples. Data are representative of $n = 4$ independent experiments.

apoptosis dependent on Bax and Bak [44], a finding that led to the suggestion that Bax and Bak [59] and the anti-apoptotic Bcl-2 proteins control apoptosis by regulating ER Ca^{2+} stores [83]. However, we found no effect of anti-apoptotic Bcl-2 proteins on m-3M3FBS-induced cell death. Therefore, it is likely that such cell death involves Bax,Bak-independent mitochondrial Ca^{2+} overload and MIMP rather than Bax,Bak-dependent MOMP. Intriguingly, high concentrations of Arachidonate behaved similarly to m-3M3FBS, inducing MIMP and a Bax,Bak-independent cell death that was delayed by CsA. Therefore, it is possible that the strength of the toxic stimulus regulates the induction of MIMP rather than MOMP and the ensuing cell death kinetics. It is likely that other observations that are difficult to interpret in terms of the mitochondrial pathway of apoptosis will be clarified through further characterization of m-3M3FBS and other inducers of Ca^{2+} overload and MIMP.

MATERIALS AND METHODS

Cell Lines

HeLa (ATCC, CCL-2), Phoenix-AMPHO (CRL-3213) and MEFs were maintained at 37 °C/5% v/v CO_2 in a humidified incubator in DMEM (GIBCO, 11971–025) supplemented with 10% FBS, 2 mM L-glutamine (GIBCO, 25030-081),100 U/mL penicillin-streptomycin (GIBCO, 15140-122), 1 mM sodium pyruvate (GIBCO, 11360-070), nonessential amino acids (GIBCO, 11140-050), and 55 μM β-mercaptoethanol (GIBCO, 21985-023). HCT 116 (ATCC, CCL-247) were maintained in McCoy's 5 A medium (ATCC 30-2207) and supplemented as above.

Experiments were performed in DMEM w/o HCO_3^-(Sigma-Aldrich, D5648) supplemented with 2% FBS, except where otherwise indicated. Light microscopy experiments were performed in DMEM w/o HCO_3^- w/o FBS, except where otherwise indicated.

siRNA transient transfection against ATP5MG (and relative NT siRNA) was performed in DMEM (GIBCO, 11971-025) supplemented as above, plus MEM vitamin solution 100X (Thermo-Fisher, 11120052) and 100 mg/L uridine (Sigma-Aldrich, U3003), as previously described [65].

Primary murine embryonic fibroblasts (MEFs) were generated by mating animals of the *ppif*$^{+/+}$ and *ppif*$^{-/-}$ genotypes and harvesting embryos at E12–E14 based on palpation. Following removal of the head and fetal liver, a single suspension was generated from the remaining parts of the embryo and plated in DMEM supplemented as above. MEFs were immortalized with the SV40 large T antigen (pBabe-Neo-SV40-LTA). MEFs *ripk3*$^{-/-}$ *mlkl*$^{-/-}$ were described previously [84]. HeLa Bax,Bak DKO were generated by CRISPR technology as previously described [7].

Cell lines were routinely tested for mycoplasma by the MycoAlert™Plus Mycoplasma Detection Kit (Lonza).

CRISPR/Cas9 genome editing

Highly edited knockout HeLa pools, KO HeLa clones, and KO MEF clones were generated using CRISPR-Cas9 technology. Briefly, 1 million HeLa or 400,000 MEFs *ripk3*$^{-/-}$ *mlkl*$^{-/-}$ cells were nucleofected (Lonza, 4D-Nucleofector™ X-unit) according to the manufacturer's recommended protocol with precomplexed ribonuclear proteins (RNPs) consisting of 100 pmol of chemically modified sgRNA (Synthego) and 33 pmol of 3XNLS *Sp*Cas9 protein (St. Jude Protein Production Shared Resource) using solution P3 and program DS-150 in small (20 μl) cuvettes. Target-specific amplicons were generated, indexed, and sequenced via NGS as previously described [85]. Resulting sequencing data was demultiplexed using index sequences, fastq files were generated, and NGS analysis was performed using CRIS.py [86]. To obtain complete KO clones, cells were dilution cloned or sorted by flow cytometry for single cells (St. Jude Flow Cytometry and Cell Sorting Shared Resource) and screened via Western blot and targeted NGS. HeLa cells were authenticated using the PowerPlex® Fusion System (Promega) performed at the Hartwell Center (St. Jude) and tested negative for mycoplasma by the MycoAlert™Plus Mycoplasma Detection Kit (Lonza). sgRNA spacer sequences and associated primers are shown in Supplementary Table 1. See Supplementary Table 2 for editing rates.

Plasmid and retroviral transduction

GCaMP3 (cyto-GCaMP3) and mito-GCaAMP3 were subclones into the pLZRS-IRES-Zeocin vector using G-CaMP3 in pEGFP-N1 (Addgene, 22692) as template; to obtain the fusion protein mito-GCaMP3, the 29 N-terminal residues of human Cytochrome C Oxidase subunit VIIIa (aa 1–29, Sequence ID: NM_004074.3) were cloned in frame at the N terminus of the GCaMP3 as mitochondrial matrix targeting sequence. ER-LAR-GECO-1 (ER-GECO) was subcloned into pMX vector (Cellbiolabs, RTV-010) using CMV-ER-LAR-GECO-1 (Addgene, 61244) as template. R-GECO-1 (cyto-GECO) was subcloned into pMX vector using R-GECO-1 sequence of the plasmid CMV-mito-R-GECO-1 (Addgene, 46021) as template. The TFAM-mCherry fusion protein was generated by cloning mCherry fluorescence protein directly on the C terminus of human transcription factor A mitochondrial (TFAM) (Sequence ID GenBank: NM_003201.2) into the pMX-IRES-Blasticidin vector (Cellbiolabs, RTV-016). pBabe Omi-mCherry vector has been described previously [87]. All BCL-2 family members cDNAs used in this study were of human origin; HA-Bcl-2, HA-Bcl-xL and HA-Mcl-1 were subcloned into the pLZRS-IRES-Zeocin [39]. The fusion protein $COX8A_{1-29}$-Cerulean was cloned adding the 29 N-terminal residues of human Cytochrome C Oxidase subunit VIIIa (aa 1–29, Sequence ID GenBank: NM_004074.3) in frame at the N terminus of the fluorescence protein Cerulean into pMX vector. The PVALB-myc fusion protein was generated by cloning the 10 amino acids Myc-Tag EQKLISEEDL on the C terminus of human parvalbumin (PVALB) (Sequence ID GenBank: BC096113.3) into the pMX-IRES-Blasticidin vector. Similarly, mito-PVALB-myc was generated by cloning the 29 N-terminal residues of human Cytochrome C Oxidase subunit VIIIa on the N terminus of PVALB-myc pMX-IRES-Blasticidin vector.

All stable cell lines were generated by retroviral transduction. Phoenix-AMPHO (amphotropic) cells (0.5×10^6 in a 10 cm dish) were transfected with retroviral constructs using Lipofectamine™ 2000 (Life Technologies, 11668027). Two days later, the virus-containing supernatant was harvested, filtered, and used to infect target cells (1×10^5 HeLa or MEFs) in presence of 5 μg/ml hexadimethrine bromide (polybrene) (Sigma-Aldrich, H9268).

Two days post infection, stable transductants were selected after adding 200 μg/mL Zeocin™ (GIBCO, R25005), or 0.5 μg/mL puromycin (Sigma-Aldrich, P8833) or were sorted by flow cytometry for GFP-, mCherry-, or Cerulean-positive cells.

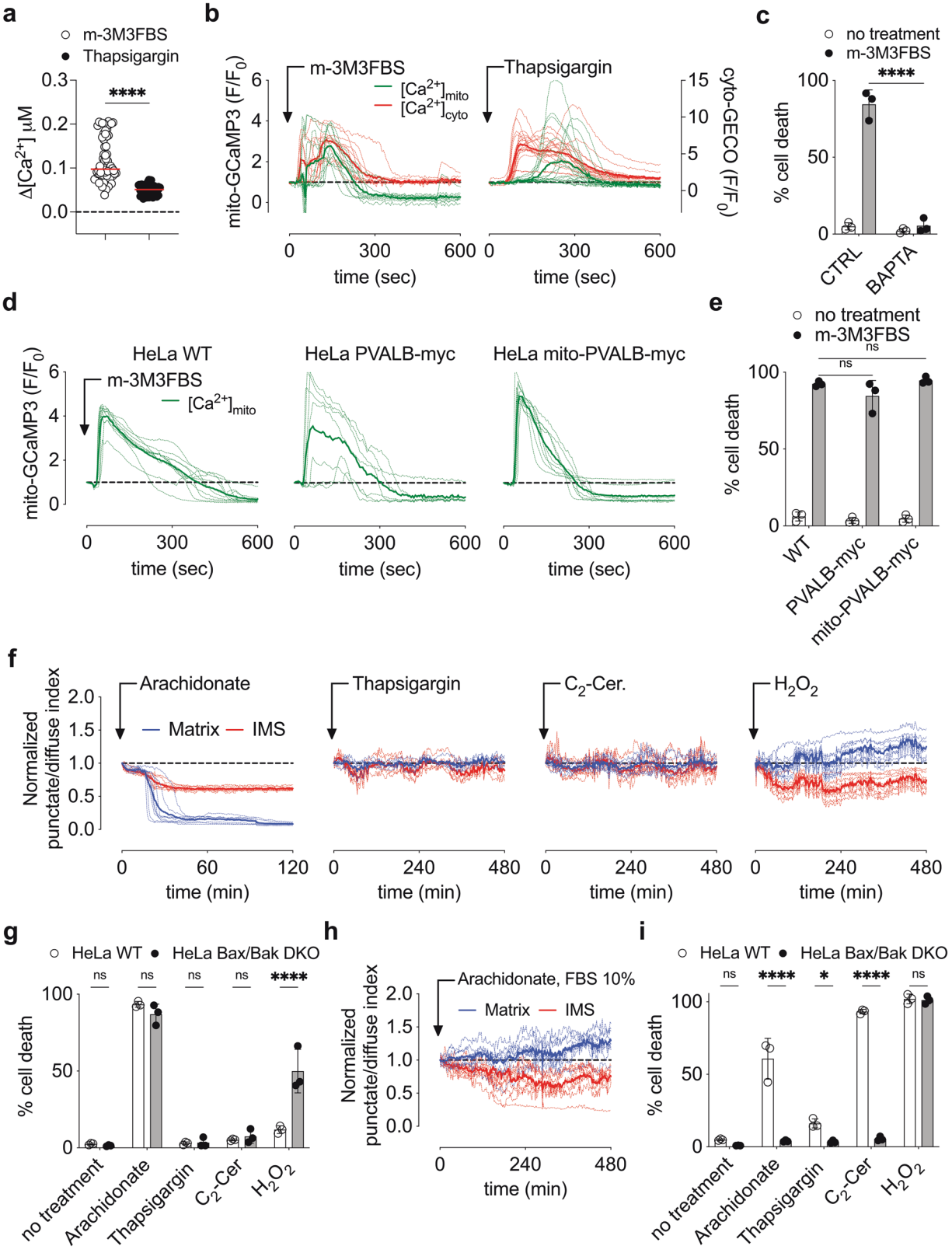

Clonogenic growth

Cells were seeded in 24 well plates (50000 per well) 24 before the assay. Then they were treated as indicated using DMEM w/o HCO_3^- (Sigma-Aldrich, D5648) supplemented with 2% FBS, in an incubator w/o CO_2. After treatment, wells were washed three times with PBS and fresh complete DMEM with 10% FBS was added. After 5–7 days in culture, the plates were gently washed with PBS and then stained with methylene blue solution (1% w/v methylene blue in a 50:50 methanol/water solution) for 30 min at room temperature. The plates were then washes with dH_2O, air dried and scanned using a document scanner.

Fig. 4 Buffering of intracellular calcium protects from m-3M3BFS induced cell death. a Intracellular Ca^{2+} spike quantification using FLIM in HeLa cells after treatment with 25 μM m-3M3FBS or 0.5 μM Thapsigargin. Each dot represents the highest $\Delta[Ca^{2+}]$ value recorded per cell. $\Delta[Ca^{2+}]$ was calculated as maximum amplitude of $[Ca^{2+}]$ oscillation from $[Ca^{2+}]_{t=0}$. Cells were pre-labeled with 4 μM of Oregon Green™ 488 BAPTA-1, AM. Data are from $n = 4$ independent experiments. **b** Mitochondrial matrix calcium (mito-GCaMP3) vs cytosolic calcium (cyto-GECO) mobilization in HeLa cells after treatment with 25 μM m-3M3FBS or 0.5 μM Thapsigargin (as fluorescence F/F_0 arbitrary units). Each dashed line represents one single cell in the field. The continuous bold line represents the mean signal from all the cells in the field. Data are representative of $n = 4$ independent experiments. **c** Cell death quantification of HeLa cells after 6 h of treatment with 25 μM m-3M3FBS in combination with 20 μM BAPTA-AM (BAPTA) using an IncuCyte imaging system. Error bars represent the SD from the mean of $n = 3$ independent experiments. **d** Mitochondrial matrix calcium quantification (mito-GCaMP3) in HeLa cells WT and expressing exogenous PVALB-myc and mito-PVALB-myc after treatment with 25 μM m-3M3FBS (as fluorescence F/F_0 arbitrary units). Each dashed line represents one single cell in the field. The continuous bolder line represents the mean signal from all the cells in the field. Data are representative of $n = 4$ independent experiments. **e** Cell death quantification of HeLa cells WT and expressing exogenous PVALB-myc and mito-PVALB-myc after 6 h of treatment with 25 μM m-3M3FBS using an IncuCyte imaging system. Error bars represent the SD from the mean of $n = 3$ independent experiments. **f** Release kinetic of IMS proteins (omi-mCherry, red) and Matrix proteins ($COX8A_{1-29}$-Cerulean, blue) in HeLa cells after treatment with 150 μM Arachidonate, 0.5 μM Thapsigargin, 40 μM C_2-cer. and 1 mM H_2O_2. Regions were drawn around cells, and punctate/diffuse indices were plotted and displayed relative to the start of the treatment (time point 0). Each dashed line represents one single cell in the field. The continuous bold line represents the mean signal from all the cells in the field for each marker. Data are representative of $n = 3$ independents experiments. **g** Cell death quantification of HeLa cells after 6 h of treatment with 150 μM Arachidonate, 0.5 μM Thapsigargin, 40 μM C_2-cer. and 1 mM H_2O_2 using an IncuCyte imaging system. Error bars represent the SD from the mean of $n = 3$ independent experiments. **h** Release kinetic of IMS proteins (omi-mCherry, red) and Matrix proteins ($COX8A_{1-29}$-Cerulean, blue) in HeLa cells after treatment with 150 μM Arachidonate in media containing 10% FBS. Regions were drawn around cells, and punctate/diffuse indices were plotted and displayed relative to the start of the treatment (time point 0). Each dashed line represents one single cell in the field. The continuous bold line represents the mean signal from all the cells in the field for each marker. Data are representative of $n = 3$ independents experiments. **i** Cell death quantification of HeLa cells after 24 h of treatment with 150 μM Arachidonate, 0.5 μM Thapsigargin, 40 μM C_2-cer. and 1 mM H_2O_2 using media containing 10% FBS in an IncuCyte imaging system. Error bars represent the SD from the mean of $n = 3$ independent experiments.

Transmission electron microscopy

HeLa cells were induced to undergo MIMP for 15 min using DMEM w/o HCO_3^- supplemented with 2% FBS, in an incubator w/o CO_2; following treatment, samples were fixed in 2.5% glutaraldehyde, 2% paraformaldehyde in 0.1 M sodium cacodylate buffer pH 7.4, and postfixed for 1.5 h in reduced 2% osmium tetroxide with 1.5% potassium ferrocyanide in 0.1 M sodium cacodylate buffer. After rinsing in buffer, samples were dehydrated through a series of graded ethanol to propylene oxide solutions, infiltrated and embedded in epoxy resin, and polymerized at 70 °C overnight. Semi-thin sections (0.5 micron) were stained with toluidine blue for light microscopic examination. Ultra-thin sections (80 nm) were cut and imaged using the Tecnai TF20 TEM with an AMT XR41 camera.

Mitochondrial permeabilization assay

24 h before the assay, 250.000 HeLa cells were plated in each well of a 6 well plate. Cells were treated as described using DMEM w/o HCO_3^- supplemented with 2% FBS, in an incubator w/o CO_2, then trypsinized, washed twice in PBS, resuspended in 40 μl of PBS + 50 μg/ml of freshly prepared Digitonin, gently vortexed and incubated on ice for 10′; after that, samples were spin for 10′ at 4 °C x 20,000 rcf. Supernatant was collected and the Pellet was solubilized in 40 μl of RIPA buffer + Protease inhibitors. Same volume of each were analyzed by SDS/PAGE and western blot.

Cell death assay

Cell death was quantified using a 2-color IncuCyte Zoom in-incubator Imaging System (Sartorius) as previously described [84]. Cell death assays in IncuCyte were performed in DMEM w/o HCO_3^- supplemented with 2% FBS, in an incubator w/o CO_2, except where otherwise indicated. % value of cell death was obtained normalized the dead cell count with the total cell count detected respectively by the uptake of 1 μg/ml of the cell impermeable dye Propidium Iodine PI (Sigma-Aldrich, P4170) and 100 nM of the cell-permeable dye Sito16 (Invitrogen S7578).

MIMP, cell death induction and chemical inhibitors

Cells were treated with the following reagents and concentrations, unless indicated otherwise: 25 μM m-3M3FBS (Tocris, 1941), 25 μM o-3M3FBS (Tocris, 1942), 1 μM U73112 (MCE, HY-13419), 50 ng/ml recombinant murine TNF-α (mTNFα) (PeproTech, 315-01 A), 100 μM Z-VAD(OMe)-FMK (zVAD) (MedChem Express, HY-16658), 5 μM ABT-737 (MCE, HY-50907), 5 μM S63845 (MCE, HY-100741), 2 μM Actinomycin D (Act.D) (Sigma-Aldrich, A1410), 2 μM Staurosporine (Staur.) (Sigma-Aldrich, S5921), 20 μM BAPTA-AM (ThermoFisher, B6769), 0.5 μM Thapsigargin (ENZO, BML-PE180-0001), 150 μM Arachidonate (20:4, n-6) (Enzo, BML-FA003-0100), 40 μM C_2-ceramide (d18:1/2:0) (Cayman, 62510), 1 mM H_2O_2 (Fisher Scientific, H325), 100 μM Histamine (Sigma-Aldrich H7125), 10 μM Xestospongin C (Cayman, 64950), 20 μM Dantrolene (Cayman, 14326), 40 μM q-VD-Oph (qVD) (MCE, HY-12305), 40 μM Calpain inhibitor III (Calp.i III) (Cayman, 14283), 2 μM jasplakinolide (Cayman, 11705), 10 μM docetaxel (Cayman, 11637), 5 μM withaferin A (W.A) (Cayman, 11352), 1–4 mM EGTA (Millipore, 324626), 20 μM Cyclosporine A (CsA) (Sigma-Aldrich, C3662), 20 μM NIM-811 (MCE, HY-P0025), 20 μM Alisporivir (MCE, HY-12559), 5–20 μM bongkrekic acid (Cayman, 19079), 2.5 μM U0126 (Cayman, 70970), 2.5 μM PD184161 (Cayman, 10012431), 2.5 μM SCH772984 (Cayman, 19166). After solubilization in DMSO, single-use aliquots of m-3M3FBS and o-3M3FBS were stored at −80 °C.

Western blotting and antibodies

Cell lysates were prepared in RIPA buffer (50 mM Tris-HCl pH 7.4, 150 mM NaCl, 1% NP40, 0.5% deoxycholic acid, 0.1% SDS, complete protease inhibitors [Roche, 11836153001] or phosphatase inhibitors [Roche, 04906837001]) for WB or NP-40 lysis buffer (0.5% NP-40, 1 mM EDTA, 150 mM NaCl, 100 mM Tris pH 7.4, complete protease Inhibitors) for affinity purification experiment. Protein concentration in cell lysates was measured by the BCA assay (Pierce) and systematically normalized before Western blotting. Samples were run on 4–12% Criterion™ XT Bis-Tris Precast Gels (Bio-Rad) and transferred to Hybond-C Extra membranes (GE Healthcare). After incubation with antibodies and the chemiluminescent substrate (homemade ECL), membranes were acquired by Chemidoc™ Touch Imaging System (Biorad) and analyzed by Image Lab software (Biorad). The following antibody were used for immunoblotting: anti-MnSOD (Cell Signaling Technology, D3X8F), anti-NDUFA9 (Invitrogen, 459100), anti-CytC (BD, 556433), anti-TOM20 (Santa Cruz Biotechnology, sc11415), anti-Mitofusin2 (MFN2) (Abcam, ab56889), anti-mCherry (Clonetech, 632543), anti-RIPK3 (Cell Signaling Technology, 95702), anti-MLKL (Abgent, AP14272b), anti-Bak (Santa Cruz Biotechnology, sc832), anti-Bax clone N-20 (Santa Cruz Biotechnology, sc493), anti-HA-tag (Sigma-Aldrich, H6908), anti-Mcl-1 (Rockland, 600–401–394), anti-Cyclophilin F (CypD) (Abcam, ab110324), anti-Parvalbumin (E8N2U) (Cell Signaling Technology, 80561), anti-Myc-tag (71D10) (Cell Signaling Technology, 2278), anti-MCU (Proteintech, 26312-1-AP), anti-LETM1 (D3) (Santa Cruz Biotechnology, sc-271234), anti-ATP5MG/ATP5L (Abcam, ab-126181), anti-β-actin clone C4 (Santa Cruz Biotechnology, sc47778). Uncropped images of the original blots are shown in Supplementary Figs. S7 and S8.

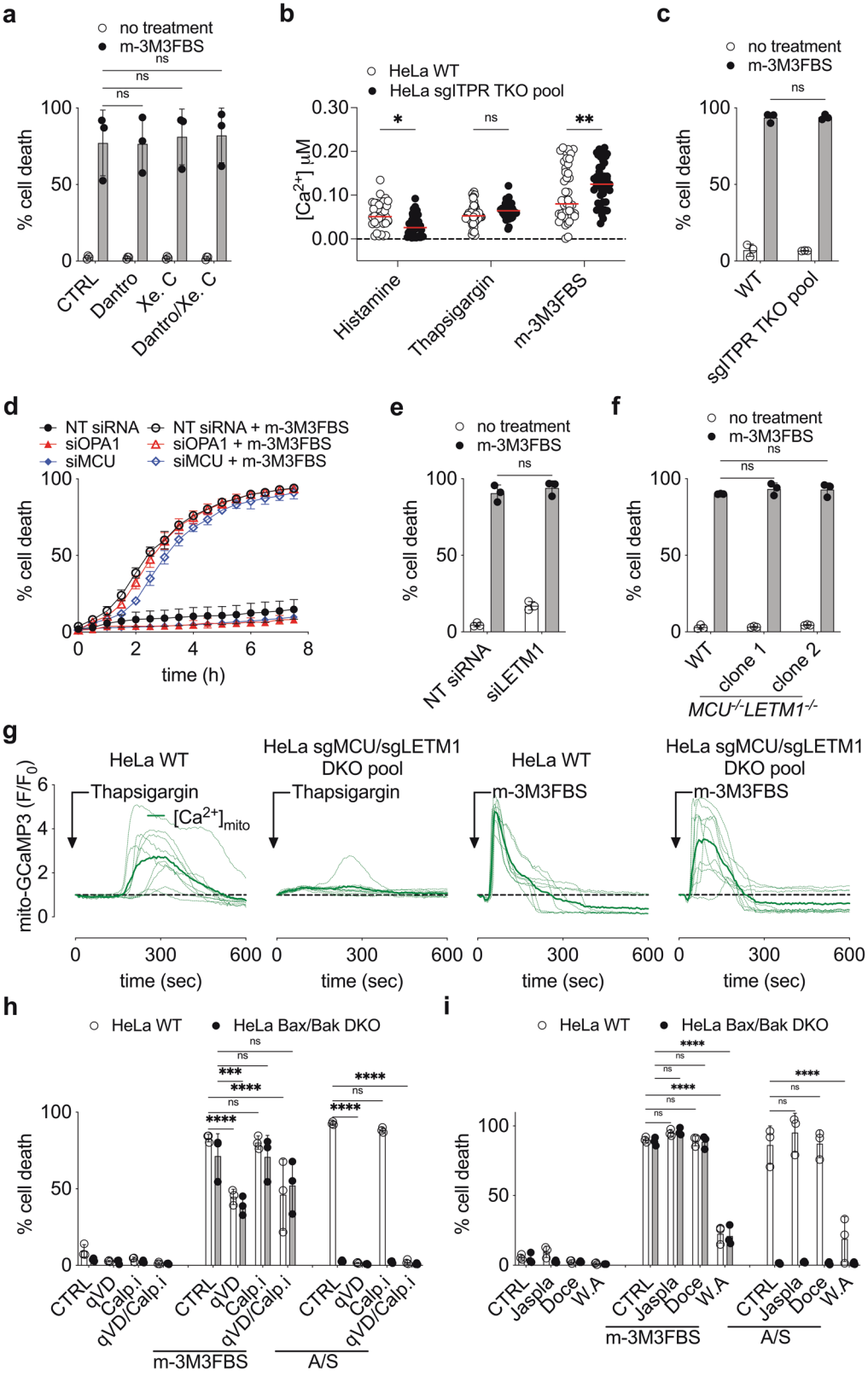
a
no treatment
m-3M3FBS
% cell death
CTRL
Dantro
Xe. C
Dantro/Xe. C
b
HeLa WT
HeLa sgITPR TKO pool
[Ca2+] µM
Histamine
Thapsigargin
m-3M3FBS
c
no treatment
m-3M3FBS
% cell death
WT
sgITPR TKO pool
d
NT siRNA
siOPA1
siMCU
NT siRNA + m-3M3FBS
siOPA1 + m-3M3FBS
siMCU + m-3M3FBS
% cell death
time (h)
e
no treatment
m-3M3FBS
% cell death
NT siRNA
siLETM1
f
no treatment
m-3M3FBS
% cell death
WT
clone 1
clone 2
MCU-/-LETM1-/-
g
HeLa WT
Thapsigargin
[Ca2+]mito
HeLa sgMCU/sgLETM1 DKO pool
Thapsigargin
HeLa WT
m-3M3FBS
HeLa sgMCU/sgLETM1 DKO pool
m-3M3FBS
mito-GCaMP3 (F/F0)
time (sec)
h
HeLa WT
HeLa Bax/Bak DKO
% cell death
CTRL
qVD
Calp.i
qVD/Calp.i
m-3M3FBS
A/S
i
HeLa WT
HeLa Bax/Bak DKO
% cell death
CTRL
Jaspla
Doce
W.A
m-3M3FBS
A/S

Fig. 5 m-3M3FBS induced MIMP and cell death does not rely on the main ER-mitochondria Ca^{2+} routes. a Cell death quantification of HeLa cells after 6 h of treatment with 25 μM m-3M3FBS in combination with 20 μM Dantrolene (Dantro) and 10 μM Xestospongin C (Xe. C) using an IncuCyte imaging system. Error bars represent the SD from the mean of $n = 3$ independent experiments. **b** Intracellular Ca^{2+} spike quantification using FLIM in HeLa WT and sgITPR TKO pool cells after treatment with 100 μM Histamine or 0.5 μM Thapsigargin or 25 μM m-3M3FBS. Each dot represents the highest $\Delta[Ca^{2+}]$ value recorded per cell. $\Delta[Ca^{2+}]$ was calculated as maximum amplitude of $[Ca^{2+}]$ oscillation from $[Ca^{2+}]_{t=0}$. Cells were pre-labeled with 4 μM of Oregon Green™ 488 BAPTA-1, AM. Data are from $n = 4$ independent experiments. **c** Cell death quantification of HeLa WT and sgITPR TKO pool cells after 6 h of treatment with 25 μM m-3M3FBS using an IncuCyte imaging system. Error bars represent the SD from the mean of $n = 3$ independent experiments. **d** Kinetic analysis of cell death in HeLa cells treated with 25 μM m-3M3FBS after silencing of MCU and OPA1 using an IncuCyte imaging system. Error bars represent the SD from the mean of triplicate samples. Data are representative of $n = 3$ independent experiments. **e** Cell death quantification of HeLa cells after 6 h of treatment with 25 μM m-3M3FBS and silencing of LETM1 using an IncuCyte imaging system. Error bars represent the SD from the mean of $n = 3$ independent experiments. **f** Cell death quantification of HeLa WT, *MCU*$^{-/-}$ *LETM1*$^{-/-}$ clone 1 and *MCU*$^{-/-}$ *LETM1*$^{-/-}$ clone 2 cells after 6 h of treatment with 25 μM m-3M3FBS using an IncuCyte imaging system. Error bars represent the SD from the mean of $n = 3$ independent experiments. **g** Mitochondrial matrix calcium quantification (mito-GCaMP3) in HeLa WT and sgMCU/sgLETM1 DKO pool after treatment with 0.5 μM Thapsigargin or 25 μM m-3M3FBS (as fluorescence F/F_0 arbitrary units). Each dashed line represents one single cell in the field. The continuous bold line represents the mean signal from all the cells in the field. Data are representative of $n = 4$ independent experiments. **h** Cell death quantification of HeLa WT and Bax,Bak DKO cells after 6 h of treatment with 25 μM m-3M3FBS or 5 μM ABT-737 + 5 μM S63845 in combination (A/S) with 40 μM qVD and/or 40 μM Calpain Inhibitor III (Calp.i). Error bars represent the SD from the mean of triplicate samples. Error bars represent the SD from the mean of $n = 3$ independent experiments. **i** Cell death quantification of HeLa WT and Bax,Bak DKO cells after 6 h of treatment with 25 μM m-3M3FBS or 5 μM ABT-737 + 5 μM S63845 in combination (A/S) with 2 μM jasplakinolide (Jaspla) or 10 μM docetaxel (Doce) or 5 μM withaferin A (W.A). Error bars represent the SD from the mean of $n = 3$ independent experiments.

Synthetic Scheme for the Preparation of Cyclosporine A—PhotoActivatable—Biotin (CsA-PA-Biotin)

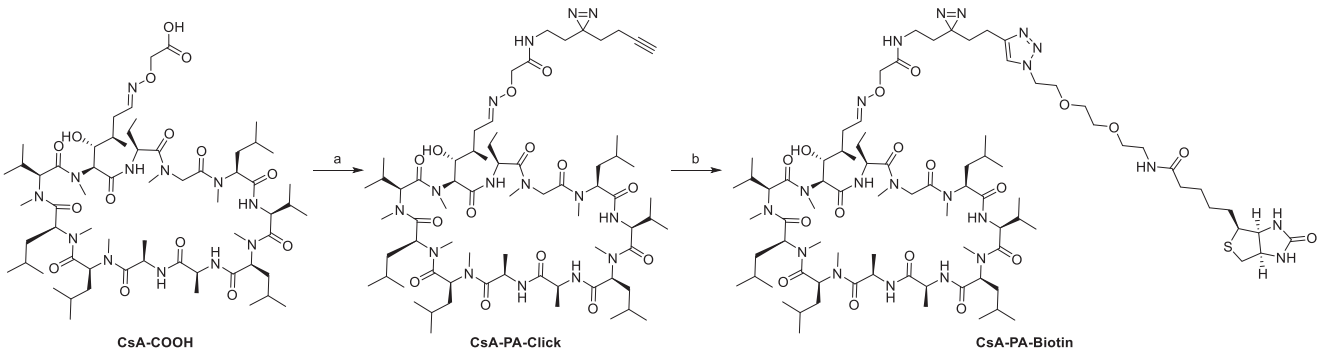

Reagents and conditions: (a) 2-(3-(but-3-yn-1-yl)−3*H*-diazirin-3-yl)ethan-1-amine, chloro-*N*,*N*,*N*′,*N*′-tetramethylformamidinium hexafluorophosphate, 1-methylimidazole, MeCN, 16 h, 75%; (b) biotin-PEG2-azide, $CuSO_4$, sodium ascorbate, *t*BuOH:H_2O (1:2), 16 h, 26%.

The synthesis of **CsA-PA-Biotin** was achieved by first preparing **CsA-COOH** as previously reported [88], followed by amide coupling with the photo-crosslinker alkyne, to obtain **CsA-PA-Click**. Click reaction with an azide functionalized biotin yielded **CsA-PA-Click**.

General methods and synthesis. Chemical reagents were purchased from commercial suppliers and were used without further purification. Automated flash chromatography was performed using the Biotage Isolera flash column system with silica gel Sfar columns. Purity was assessed using UPLC-MS (Acquity PDA detector, Acquity SQ detector and Acquity UPLC BEH-C18 column 1.7 μm, 2.1 × 50 mm [Waters Corp.]) with mobile phase of 0.1% formic acid in H_2O and acetonitrile. The mass spectrometer was operated in positive-ion and negative-ion modes with electrospray ionization and data were acquired using Masslynx, version 4.1.

Synthesis of CsA-PA-Click. Chloro-*N*,*N*,*N*′,*N*′-tetramethylformamidinium hexafluorophosphate (44 mg, 0.158 mmol) was added to a stirring solution of **CsA-COOH** (100 mg, 0.079 mmol), 2-(3-(but-3-yn-1-yl)−3*H*-diazirin-3-yl) ethan-1-amine (13 mg, 0.095 mmol), and 1-methylimidazole (25 μL, 0.317 mmol), in MeCN (1.5 mL). After 16 h the reaction mixture was added to water (10 mL) and extracted with EtOAc (2 × 10 mL). The combined organic layers were washed with saturated brine, dried over anhydrous Na_2SO_4, filtered, and concentrated. The crude mixture was purified by flash column chromatography (Biotage Isolera, 10 g Sfar column, 0–8% CH_2Cl_2:MeOH) to give the desired product (82 mg, 75%). LC-MS (ESI): *m/z*, [M + H] calc. for $C_{69}H_{120}N_{15}O_{14}$, 1382.91; obs. 1383.58.

Synthesis of CsA-PA-Biotin. Sodium ascorbate (1 M, 165 μL, 0.165 mmol) was added to a solution of **CsA-PA-Click** (57 mg, 0.041 mmol), biotin-PEG2-azide (33 mg, 0.082 mmol), and $CuSO_4$ (1 M, 165 μL, 0.165 mmol), in *t*BuOH:H_2O (1:2) (3 mL). After 16 h, the reaction mixture was diluted with MeCN and purify by reverse-phase chromatography to give the desired product (19 mg, 26%). LC-MS (ESI): *m/z*, [M + H] calc. for $C_{85}H_{148}N_{21}O_{18}S$, 1783.10; obs. 1783.81.

CsA-PA-Biotin affinity purification

CsA-PA-Biotin affinity purification was performed as partial modification of a previously described protocol (Gloeckner et al., 2009). Briefly, samples were collected after 1 h preincubation with 20 μM CsA-PA-Biotin and 4 h incubation with 25 μM of m-3M3FBS (or 90 min of 50 μM m-3M3FBS), washed twice with PBS, resuspended at a concentration of 6×10^6 cells x ml in 2 ml of PBS and exposed to 365 nm UV light for 20 min at 4 °C with an 3 UV lamp (Thermo Fisher, 95034) to induce activation of the diazirine group (that reacts efficiently with any amino acid side chain or peptide backbone upon activation with long-wave UV light (330–370 nm)). Cells were then lysed in NP-40 lysis buffer (see above), and clarified lysates were precipitated with Strep-Tactin® XT Superflow® (IBA Lifesciences, 2-4010-010), washed in cell lysis buffer, and eluted with BXT buffer (IBA-Lifesciences, 2-1042-025). The eluate was concentrated using Amicon® Ultra-15 and Amicon® Ultra-0.5, 10 kDa Centrifugal Filter Units (Millipore, UFC901024 and UFC501096).

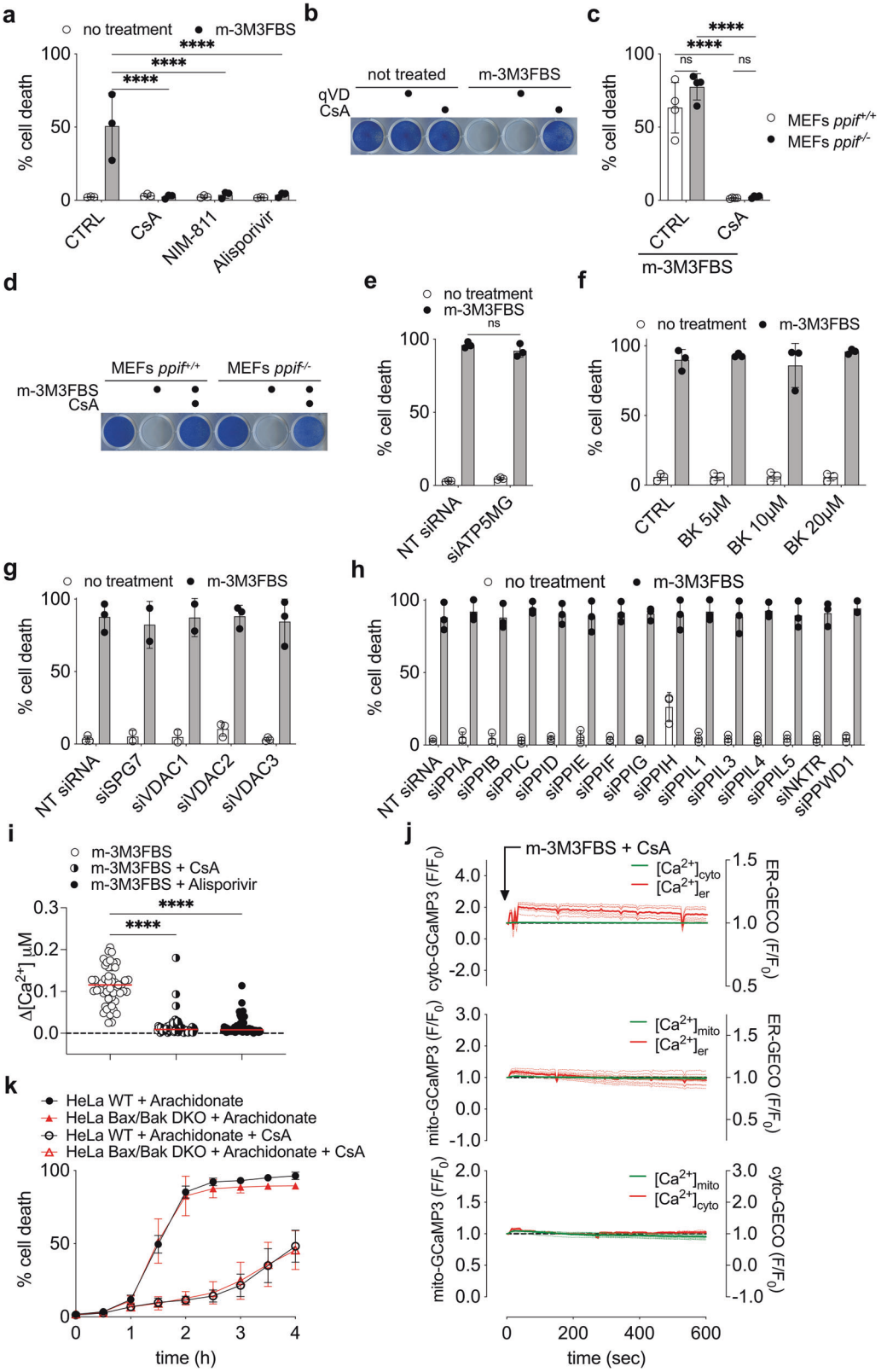

Mass spectrometry analysis

CsA-PA-Biotin-binding proteins were purified by affinity purification, as described above, and briefly subjected to SDS-PAGE, in-gel digestion and mass spectrometry analysis. Briefly, after staining with GelCode Blue (Pierce, 24590), each gel lane was excised into 4 bands and subjected to dithiothreitol reduction, iodoacetamide alkylation, and in-gel digestion (12.5 ng/μL trypsin overnight). Resulting tryptic peptides were concentrated, loaded on a self-packed column (75 μm × 15 cm with 1.9 μm C18 resin from Dr. Maisch GmbH). Peptides were analyzed in a 60 min gradient at 250 nL/min flow rate (buffer A: 0.2% formic acid, 5% DMSO; buffer B:

Fig. 6 MIMP is inhibited by Cyclosporine A independently of Cyclophilins. a Cell death quantification of HeLa cells after 6 h of treatment with 25 μM m-3M3FBS in combination with 20 μM Cyclosporin A (CsA) or 20 μM NIM-811 or 20 μM Alisporivir using an IncuCyte imaging system. Error bars represent the SD from the mean of $n = 3$ independent experiments. **b** Clonogenic survival of HeLa cells after treatment with 25 μM m-3M3FBS in combination with 40 μM qVD or 20 μM CsA. Data are representative of $n = 4$ independent experiments. **c** Cell death quantification of MEFs *ppif*$^{+/+}$ and *ppif*$^{-/-}$ after 6 h of treatment with 25 μM m-3M3FBS in combination with 20 μM CsA using an IncuCyte imaging system. Error bars represent the SD from the mean of $n = 3$ independent experiments. **d** Clonogenic survival of MEFs *ppif*$^{+/+}$ and *ppif*$^{-/-}$ after treatment with 25 μM m-3M3FBS in combination with 20 μM CsA. Data are representative of $n = 3$ independent experiments. **e** Cell death quantification of HeLa cells after 6 h of treatment with 25 μM m-3M3FBS and silencing of ATP5MG, using an IncuCyte imaging system. Error bars represent the SD from the mean of $n = 3$ independent experiments. **f** Cell death quantification of HeLa cells after 6 h of treatment with 25 μM m-3M3FBS in combination with different concentrations of bongkrekic acid (BK), as indicated in the Figure, using an IncuCyte imaging system. Error bars represent the SD from the mean of $n = 3$ independent experiments. No statistically significant differences were observed between treated samples when compared to CTRL. **g** Cell death quantification of HeLa cells after 6 h of treatment with 25 μM m-3M3FBS and silencing of SPG7, VDAC1, VDAC2 and VDAC3, using an IncuCyte imaging system. Error bars represent the SD from the mean of $n \geq 2$ independent experiments. No statistically significant differences were observed between treated samples when compared to NT siRNA. **h** Cell death in HeLa cells after 6 h of treatment with 25 μM m-3M3FBS and silencing of the peptidylprolyl isomerase (PPIase) family members, as reported in Supp. Table 4, using an IncuCyte imaging system. Error bars represent the SD from the mean of triplicate samples. Error bars represent the SD from the mean of $n = 3$ independent experiments. No statistically significant differences were observed between treated samples when compared to NT siRNA. **i** Intracellular Ca^{2+} spike quantification using FLIM in HeLa cells after treatment with 25 μM m-3M3FBS in combination with 20 μM CsA or 20 μM Alisporivir. Each dot represents the highest $\Delta[Ca^{2+}]$ value recorded for each cell. $\Delta[Ca^{2+}]$ was calculated as maximum amplitude of $[Ca^{2+}]$ oscillation from $[Ca^{2+}]_{t=0}$. Cells were pre-labeled with 4 μM of Oregon Green™ 488 BAPTA-1, AM. Data are from $n = 4$ independent experiments. **j** Intracellular calcium mobilization in HeLa cells after treatment with 25 μM m-3M3FBS and 20 μM CsA at single cell level, to compare to Fig. 1d (as fluorescence F/F_0 arbitrary units). Upper panel: cytosolic calcium (cyto-GCaMP3) vs ER lumen calcium (ER-GECO); middle panel mitochondrial matrix calcium (mito-GCaMP3) vs ER lumen calcium (ER-GECO); lower panel matrix mitochondrial calcium (mito-GCaMP3) vs cytosolic calcium (cyto-GECO). Each dashed line represents one single cell in the field. The continuous bold line represents the mean signal from all the cells in the field. Data are representative of $n = 4$ independent experiments. **k** Kinetic analysis of cell death in HeLa cells treated with 150 μM Arachidonate in combination with 20 μM CsA. Error bars represent the SD from the mean of triplicate samples. Data are representative of $n = 3$ independent experiments.

buffer A plus 65% AcN) on a Q Exactive HF Orbitrap MS (Thermo Fisher Scientific). The MS spectra were collected in the followed parameters: MS1-60,000 resolution, 350–1600 m/z scan range, 1×10^6 AGC, and 50 ms maximal ion time and MS2-20 data-dependent MS2 scans, 60,000 resolution, 1×10^5 AGC, 125 ms maximal ion time, 1.6 m/z isolation window with 0.2 m/z offset, HCD, 35 specified normalized collision energy (NCE), and 8 s dynamic exclusion. Database searches were performed for peptide/protein identification (protein false discovery rate below 1%). Finally, the total number of protein-spectrum matches, namely spectral counts (SC), assigned to individual proteins reflects their relative abundance in the samples.

Transient transfection

siRNA transient transfection was performed over 48 h Lipofectamine™ RNAiMAX transfection reagents (Invitrogen, 13778075), as per the manufacturers' instructions. All siRNA oligos used were ON-TARGET plus siRNA pools of 4 oligos purchased from Dharmacon, as specified in Table S5.

Real-time PCR

Total RNA for real-time PCR was extracted and purified using the RNeasy Mini Kit (QIAGEN, 74104). Reverse transcription reactions were performed with M-MLV reverse transcriptase (Invitrogen, 28025013), following the standard protocol using random hexamers (IDT, 51-01-18-26). Real-time PCR was performed using SYBR Green technology (Invitrogen, 4309155) in 7500 Fast Real-Time PCR System (Applied Biosystems). PCR conditions were 50 °C for 2 min, 95 °C for 10 min, and 45 cycles of 95 °C for 15 s and 60 °C for 1 min. mRNA expression was normalized against β-actin, allowing comparison of mRNA levels. Primers used in this study were acquired by IDT and are listed in Table S6.

Cell Imaging and fluorescent probes

Live-cell microscopy analyses were performed using a Marianas spinning disc laser scanning confocal system (Intelligent Imaging Innovations) built on an AxioObserverZ.1 inverted microscope stand (Carl Zeiss Microscopy) equipped with environmental control and a 63× 1.4 NA objective. Phosphatidylserine exposure and initial loss of plasma membrane integrity was visualized by Annexin V-Pacific Blue™ (AV-PacBlue) (Invitrogen, A35122). Mitochondrial transmembrane potential was recorded using 200 nM of Tetramethylrhodamine, Ethyl Ester, Perchlorate (TMRE) (ThermoFisher, T669) Appropriate laser lines were used to detect GFP- and mCherry-tagged fluorescent proteins, with images captured by an Evolve EMCCD camera (Photometrics). Image acquisition and analysis were performed using Slidebook software (Intelligent Imaging Innovations). Time-lapsed imaging using wide-field illumination was performed using a Nikon Ti-E microscope equipped with an Apo 60× 1.4 NA objective and appropriate dichroic mirror and filters for illumination and detection of GFP and RFP-tagged proteins. Images were acquired using an Andor DU-897 EMCCD camera and Nikon Elements software.

Fluorescence lifetime imaging

Live imaging was performed using an AxioObserver Z.1 inverted microscope (Carl Zeiss Inc) and Marianas confocal microscope (intelligent Imaging Innovations) equipped with a CSU-W SoRa spinning disk. Oregon Green BAPTA-1, AM (ThermoFisher, O6807)-labelled cells were imaged using a 40×1.3NA EC Plan-Neoflaur objective, a direct-modulated 488 nm solid state laser and modulated image intensifier (Lambert Instruments), with fluorescence collected onto an HQ2 EMCCD camera. Calibration of the fluorescence lifetime was facilitated using Rhodamine 110 in water as a reference. Determination of calcium concentration was performed using the Oregon green BAPTA-1 hexapotassium salt (ThermoFisher, O6806) and a calcium calibration kit (Biotium, 5100).

Super-resolution structured illumination microscopy

Cells were cultured on thickness #1.5 cover slips prior to treatment and subsequent fixation with 4% paraformaldehyde. Samples were permeabilized with 0.1% T-100 and blocked with 2% bovine serum albumin in PBS for 20 min prior to incubation with goat-anti-mCherry (Biorbyt, orb11618) and rabbit anti-Tom20 (Abcam, ab186735) overnight at 4 °C. Primary antibodies were washed and detected with AF568-conjugated Donkey anti-Goat (ThermoFisher, A-11057) and AF647-conjugated Donkey anti-Rabbit (ThermoFisher, A-31573) secondary antibodies, prior to washing and mounting with Prolong Glass antifade mountant (ThermoFisher, P36984). Images were acquired using an Elyra PS.1 microscope (Carl Zeiss Inc) equipped with a Plan-Apochromat 100 × 1.46NA oil objective and 561 and 642 nm laser lines. Images were processed for structured illumination and deconvolution using Zen Black software and were subsequently analyzed and exported using Imaris software (Bitplane).

Stability of m-3M3FBS in DMEM media in the presence and absence of CsA

To observe the stability of m-3M3FBS in the presence and absence of CsA, 25 μM m-3M3FBS was incubated in DMEM media in the presence of 0, 20, and 40 μM CsA, at 37 °C. At time 0, 30 min, 1 h, 2 h, and 4 h, an aliquot of the solution was spun down and the supernatant analyzed by UPLC-MS (Acquity PDA detector, Acquity SQ detector and Acquity UPLC BEH-C18 column 1.7 μm, 2.1 × 50 mm [Waters Corp.]).

Metabolic phenotyping

Extracellular acidification rate (ECAR) and oxygen consumption rate (OCR) were measured using the Seahorse XFe bioanalyzer. 1.5×10^4 HeLa cells per well were plated onto h-Fibronectin coated seahorse 96 well plates and incubate for 6 h with complete DMEM at 37 °C/5% v/v CO_2 in a humidified incubator; 1 h before the experiment cells were washed with PBS and fresh Seahorse XF base medium (Agilent, 102353-100); media was supplemented with 2 mM Glutamine (for ECAR and OCR quantification), and 1 mM NaPyruvate (for OCR quantification); then the plate was preincubated at 37 °C for 1 h in the absence of CO_2. OCR and ECAR were measured under basal conditions and after the addition of the following substrates/drugs: 10 mM glucose (Sigma, G7021), 25 μM m-3M3FBS, 0.5 μM rotenone (Calbiochem, 557368) + 0.5 μM antimycin A (Sigma, A8674) and 50 mM 2-deoxy-glucose (Sigma, D8375) as indicated in figure legend. Because of the low solubility in basic media, for m-3M3FBS administration, Seahorse XFe96 Sensor Cartridge port B was loaded with a 10x solution of 80%/20% v/v of DMSO/Media. Measurements were taken using a 96 well Extracellular Flux Analyzer (SeahorseBioscience).

Statistical analysis

Data were shown as means ± SD except where otherwise indicated; please refer to the legend of the figures for description of number of replicates and repeats of individual experiments. No statistical tests were used to estimate sample size. Data were plotted and analyzed with GraphPad Prism 9.0 software (GraphPad Software). Statistical significance was determined using a *two-way ANOVA* followed by Sidak's multiple comparisons test. The threshold for significance were denoted as * where $p < 0.05$; ** where $p < 0.01$; *** where $p < 0.001$; and N.S. = not significant.

DATA AVAILABILITY

All relevant data are available from the authors upon reasonable request.

REFERENCES

1. Tait SW, Green DR. Mitochondrial regulation of cell death. Cold Spring Harb Perspect Biol. 2013;5.
2. Green DR, Fitzgerald P. Just So Stories about the Evolution of Apoptosis. Curr Biol. 2016;26:R620–r7.
3. Green DR, Llambi F. Cell Death Signaling. Cold Spring Harb Perspect Biol. 2015;7.
4. Bossy-Wetzel E, Newmeyer DD, Green DR. Mitochondrial cytochrome c release in apoptosis occurs upstream of DEVD-specific caspase activation and independently of mitochondrial transmembrane depolarization. Embo J. 1998;17:37–49.
5. Waterhouse NJ, Goldstein JC, von Ahsen O, Schuler M, Newmeyer DD, Green DR. Cytochrome c maintains mitochondrial transmembrane potential and ATP generation after outer mitochondrial membrane permeabilization during the apoptotic process. J Cell Biol. 2001;153:319–28.
6. McArthur K, Whitehead LW, Heddleston JM, Li L, Padman BS, Oorschot V, et al. BAK/BAX macropores facilitate mitochondrial herniation and mtDNA efflux during apoptosis. Science. 2018;359.
7. Riley JS, Quarato G, Cloix C, Lopez J, O'Prey J, Pearson M, et al. Mitochondrial inner membrane permeabilisation enables mtDNA release during apoptosis. Embo J. 2018;37.
8. Haworth RA, Hunter DR. The Ca2+-induced membrane transition in mitochondria. II. Nature of the Ca2+ trigger site. Arch Biochem Biophys. 1979;195:460–7.
9. Utsumi K. Mitochondrial swelling induced by Ca2+ and inorganic phosphate and its related phenomena. Acta Med Okayama. 1964;18:189–205.
10. Lehninger AL. Water uptake and extrusion by mitochondria in relation to oxidative phosphorylation. Physiol Rev. 1962;42:467–517.
11. Hunter DR, Haworth RA, Southard JH. Relationship between configuration, function, and permeability in calcium-treated mitochondria. J Biol Chem. 1976;251:5069–77.
12. Bernardi P, Rasola A, Forte M, Lippe G. The Mitochondrial Permeability Transition Pore: Channel Formation by F-ATP Synthase, Integration in Signal Transduction, and Role in Pathophysiology. Physiol Rev. 2015;95:1111–55.
13. Crompton M, Ellinger H, Costi A. Inhibition by cyclosporin A of a Ca2+-dependent pore in heart mitochondria activated by inorganic phosphate and oxidative stress. Biochem J. 1988;255:357–60.
14. Rosenwirth B, Billich A, Datema R, Donatsch P, Hammerschmid F, Harrison R, et al. Inhibition of human immunodeficiency virus type 1 replication by SDZ NIM 811, a nonimmunosuppressive cyclosporine analog. Antimicrob Agents Chemother. 1994;38:1763–72.
15. Hansson MJ, Mattiasson G, Månsson R, Karlsson J, Keep MF, Waldmeier P, et al. The nonimmunosuppressive cyclosporin analogs NIM811 and UNIL025 display nanomolar potencies on permeability transition in brain-derived mitochondria. J Bioenerg Biomembr. 2004;36:407–13.
16. Gomez L, Thibault H, Gharib A, Dumont JM, Vuagniaux G, Scalfaro P, et al. Inhibition of mitochondrial permeability transition improves functional recovery and reduces mortality following acute myocardial infarction in mice. Am J Physiol Heart Circ Physiol. 2007;293:H1654–61.
17. Handschumacher RE, Harding MW, Rice J, Drugge RJ, Speicher DW. Cyclophilin: a specific cytosolic binding protein for cyclosporin A. Science. 1984;226:544–7.
18. Basso E, Fante L, Fowlkes J, Petronilli V, Forte MA, Bernardi P. Properties of the permeability transition pore in mitochondria devoid of Cyclophilin D. J Biol Chem. 2005;280:18558–61.
19. Marzo I, Brenner C, Zamzami N, Susin SA, Beutner G, Brdiczka D, et al. The permeability transition pore complex: a target for apoptosis regulation by caspases and bcl-2-related proteins. J Exp Med. 1998;187:1261–71.
20. Eliseev RA, Malecki J, Lester T, Zhang Y, Humphrey J, Gunter TE. Cyclophilin D interacts with Bcl2 and exerts an anti-apoptotic effect. J Biol Chem. 2009;284:9692–9.
21. Nakagawa T, Shimizu S, Watanabe T, Yamaguchi O, Otsu K, Yamagata H, et al. Cyclophilin D-dependent mitochondrial permeability transition regulates some necrotic but not apoptotic cell death. Nature. 2005;434:652–8.
22. Baines CP, Kaiser RA, Purcell NH, Blair NS, Osinska H, Hambleton MA, et al. Loss of cyclophilin D reveals a critical role for mitochondrial permeability transition in cell death. Nature. 2005;434:658–62.
23. Bae YS, Lee TG, Park JC, Hur JH, Kim Y, Heo K, et al. Identification of a compound that directly stimulates phospholipase C activity. Mol Pharmacol. 2003;63:1043–50.
24. Lee YN, Lee HY, Kim JS, Park C, Choi YH, Lee TG, et al. The novel phospholipase C activator, m-3M3FBS, induces monocytic leukemia cell apoptosis. Cancer Lett. 2005;222:227–35.
25. Jung EM, Lee TJ, Park JW, Bae YS, Kim SH, Choi YH, et al. The novel phospholipase C activator, m-3M3FBS, induces apoptosis in tumor cells through caspase activation, down-regulation of XIAP and intracellular calcium signaling. Apoptosis. 2008;13:133–45.
26. Agronskaia AV, Tertoolen L, Gerritsen HC. Fast fluorescence lifetime imaging of calcium in living cells. J Biomed Opt. 2004;9:1230–7.
27. Tian L, Hires SA, Mao T, Huber D, Chiappe ME, Chalasani SH, et al. Imaging neural activity in worms, flies and mice with improved GCaMP calcium indicators. Nat Methods. 2009;6:875–81.
28. Dana H, Mohar B, Sun Y, Narayan S, Gordus A, Hasseman JP, et al. Sensitive red protein calcium indicators for imaging neural activity. Elife. 2016;5.
29. Llambi F, Moldoveanu T, Tait SW, Bouchier-Hayes L, Temirov J, McCormick LL, et al. A unified model of mammalian BCL-2 protein family interactions at the mitochondria. Mol Cell. 2011;44:517–31.
30. Krjukova J, Holmqvist T, Danis AS, Akerman KE, Kukkonen JP. Phospholipase C activator m-3M3FBS affects Ca2+ homeostasis independently of phospholipase C activation. Br J Pharmacol. 2004;143:3–7.
31. Shi J, Zhao Y, Wang K, Shi X, Wang Y, Huang H, et al. Cleavage of GSDMD by inflammatory caspases determines pyroptotic cell death. Nature. 2015;526:660–5.
32. Wang Y, Gao W, Shi X, Ding J, Liu W, He H, et al. Chemotherapy drugs induce pyroptosis through caspase-3 cleavage of a gasdermin. Nature. 2017;547:99–103.
33. Rogers C, Fernandes-Alnemri T, Mayes L, Alnemri D, Cingolani G, Alnemri ES. Cleavage of DFNA5 by caspase-3 during apoptosis mediates progression to secondary necrotic/pyroptotic cell death. Nat Commun. 2017;8:14128.
34. Lee GS, Subramanian N, Kim AI, Aksentijevich I, Goldbach-Mansky R, Sacks DB, et al. The calcium-sensing receptor regulates the NLRP3 inflammasome through Ca2+ and cAMP. Nature. 2012;492:123–7.
35. Kaiser WJ, Upton JW, Long AB, Livingston-Rosanoff D, Daley-Bauer LP, Hakem R, et al. RIP3 mediates the embryonic lethality of caspase-8-deficient mice. Nature. 2011;471:368–72.
36. Oberst A, Dillon CP, Weinlich R, McCormick LL, Fitzgerald P, Pop C, et al. Catalytic activity of the caspase-8-FLIP(L) complex inhibits RIPK3-dependent necrosis. Nature. 2011;471:363–7.
37. Sun L, Wang H, Wang Z, He S, Chen S, Liao D, et al. Mixed lineage kinase domain-like protein mediates necrosis signaling downstream of RIP3 kinase. Cell. 2012;148:213–27.
38. Chipuk JE, Moldoveanu T, Llambi F, Parsons MJ, Green DR. The BCL-2 family reunion. Mol Cell. 2010;37:299–310.
39. Llambi F, Wang YM, Victor B, Yang M, Schneider DM, Gingras S, et al. BOK Is a Non-canonical BCL-2 Family Effector of Apoptosis Regulated by ER-Associated Degradation. Cell. 2016;165:421–33.
40. Zou H, Henzel WJ, Liu X, Lutschg A, Wang X. Apaf-1, a human protein homologous to C. elegans CED-4, participates in cytochrome c-dependent activation of caspase-3. Cell. 1997;90:405–13.
41. Pinton P, Ferrari D, Magalhães P, Schulze-Osthoff K, Di Virgilio F, Pozzan T, et al. Reduced loading of intracellular Ca(2+) stores and downregulation of capacitative Ca(2+) influx in Bcl-2-overexpressing cells. J Cell Biol. 2000;148:857–62.

42. Foyouzi-Youssefi R, Arnaudeau S, Borner C, Kelley WL, Tschopp J, Lew DP, et al. Bcl-2 decreases the free Ca2+ concentration within the endoplasmic reticulum. Proc Natl Acad Sci USA. 2000;97:5723–8.
43. Deniaud A, Sharaf el dein O, Maillier E, Poncet D, Kroemer G, Lemaire C, et al. Endoplasmic reticulum stress induces calcium-dependent permeability transition, mitochondrial outer membrane permeabilization and apoptosis. Oncogene. 2008;27:285–99.
44. Scorrano L, Oakes SA, Opferman JT, Cheng EH, Sorcinelli MD, Pozzan T, et al. BAX and BAK regulation of endoplasmic reticulum Ca2+: a control point for apoptosis. Science. 2003;300:135–9.
45. Butera G, Vecellio Reane D, Canato M, Pietrangelo L, Boncompagni S, Protasi F, et al. Parvalbumin affects skeletal muscle trophism through modulation of mitochondrial calcium uptake. Cell Rep. 2021;35:109087.
46. Guerra MT, Fonseca EA, Melo FM, Andrade VA, Aguiar CJ, Andrade LM, et al. Mitochondrial calcium regulates rat liver regeneration through the modulation of apoptosis. Hepatology. 2011;54:296–306.
47. Mendes TB, Nozima BH, Budu A, de Souza RB, Braga Catroxo MH, Delcelo R, et al. PVALB diminishes [Ca2+] and alters mitochondrial features in follicular thyroid carcinoma cells through AKT/GSK3β pathway. Endocr Relat Cancer. 2016;23:769–82.
48. Obeid LM, Linardic CM, Karolak LA, Hannun YA. Programmed cell death induced by ceramide. Science. 1993;259:1769–71.
49. Szalai G, Krishnamurthy R, Hajnóczky G. Apoptosis driven by IP(3)-linked mitochondrial calcium signals. Embo J. 1999;18:6349–61.
50. Scorrano L, Penzo D, Petronilli V, Pagano F, Bernardi P. Arachidonic acid causes cell death through the mitochondrial permeability transition. Implications for tumor necrosis factor-alpha aopototic signaling. J Biol Chem. 2001;276:12035–40.
51. Hockenbery DM, Oltvai ZN, Yin XM, Milliman CL, Korsmeyer SJ. Bcl-2 functions in an antioxidant pathway to prevent apoptosis. Cell. 1993;75:241–51.
52. Wolf LA, Laster SM. Characterization of arachidonic acid-induced apoptosis. Cell Biochem Biophys. 1999;30:353–68.
53. Martin SJ, Takayama S, McGahon AJ, Miyashita T, Corbeil J, Kolesnick RN, et al. Inhibition of ceramide-induced apoptosis by Bcl-2. Cell Death Differ. 1995;2:253–7.
54. Tochigi M, Inoue T, Suzuki-Karasaki M, Ochiai T, Ra C, Suzuki-Karasaki Y. Hydrogen peroxide induces cell death in human TRAIL-resistant melanoma through intracellular superoxide generation. Int J Oncol. 2013;42:863–72.
55. Troyano A, Sancho P, Fernández C, de Blas E, Bernardi P, Aller P. The selection between apoptosis and necrosis is differentially regulated in hydrogen peroxide-treated and glutathione-depleted human promonocytic cells. Cell Death Differ. 2003;10:889–98.
56. Ando H, Hirose M, Mikoshiba K. Aberrant IP(3) receptor activities revealed by comprehensive analysis of pathological mutations causing spinocerebellar ataxia 29. Proc Natl Acad Sci USA. 2018;115:12259–64.
57. Baughman JM, Perocchi F, Girgis HS, Plovanich M, Belcher-Timme CA, Sancak Y, et al. Integrative genomics identifies MCU as an essential component of the mitochondrial calcium uniporter. Nature. 2011;476:341–5.
58. De Stefani D, Raffaello A, Teardo E, Szabo I, Rizzuto R. A forty-kilodalton protein of the inner membrane is the mitochondrial calcium uniporter. Nature. 2011;476:336–40.
59. Pan X, Liu J, Nguyen T, Liu C, Sun J, Teng Y, et al. The physiological role of mitochondrial calcium revealed by mice lacking the mitochondrial calcium uniporter. Nat Cell Biol. 2013;15:1464–72.
60. Kushnareva YE, Gerencser AA, Bossy B, Ju WK, White AD, Waggoner J, et al. Loss of OPA1 disturbs cellular calcium homeostasis and sensitizes for excitotoxicity. Cell Death Differ. 2013;20:353–65.
61. Jiang D, Zhao L, Clapham DE. Genome-wide RNAi screen identifies Letm1 as a mitochondrial Ca2+/H+ antiporter. Science. 2009;326:144–7.
62. Nelson WJ, Traub P. Intermediate (10 nm) filament proteins and the Ca2+-activated proteinase specific for vimentin and desmin in the cells from fish to man: an example of evolutionary conservation. J Cell Sci. 1982;57:25–49.
63. Davis MA, Fairgrieve MR, Den Hartigh A, Yakovenko O, Duvvuri B, Lood C, et al. Calpain drives pyroptotic vimentin cleavage, intermediate filament loss, and cell rupture that mediates immunostimulation. Proc Natl Acad Sci USA. 2019;116:5061–70.
64. Neginskaya MA, Solesio ME, Berezhnaya EV, Amodeo GF, Mnatsakanyan N, Jonas EA, et al. ATP Synthase C-Subunit-Deficient Mitochondria Have a Small Cyclosporine A-Sensitive Channel, but Lack the Permeability Transition Pore. Cell Rep. 2019;26:11–7.e2.
65. Carrer A, Tommasin L, Šileikytė J, Ciscato F, Filadi R, Urbani A, et al. Defining the molecular mechanisms of the mitochondrial permeability transition through genetic manipulation of F-ATP synthase. Nat Commun. 2021;12:4835.
66. Henderson PJ, Lardy HA. Bongkrekic acid. An inhibitor of the adenine nucleotide translocase of mitochondria. J Biol Chem. 1970;245:1319–26.
67. Shimizu S, Shinohara Y, Tsujimoto Y. Bax and Bcl-xL independently regulate apoptotic changes of yeast mitochondria that require VDAC but not adenine nucleotide translocator. Oncogene. 2000;19:4309–18.
68. Madesh M, Hajnóczky G. VDAC-dependent permeabilization of the outer mitochondrial membrane by superoxide induces rapid and massive cytochrome c release. J Cell Biol. 2001;155:1003–15.
69. Cesura AM, Pinard E, Schubenel R, Goetschy V, Friedlein A, Langen H, et al. The voltage-dependent anion channel is the target for a new class of inhibitors of the mitochondrial permeability transition pore. J Biol Chem. 2003;278:49812–8.
70. Shanmughapriya S, Rajan S, Hoffman NE, Higgins AM, Tomar D, Nemani N, et al. SPG7 Is an Essential and Conserved Component of the Mitochondrial Permeability Transition Pore. Mol Cell. 2015;60:47–62.
71. Hu G, Wang K, Groenendyk J, Barakat K, Mizianty MJ, Ruan J, et al. Human structural proteome-wide characterization of Cyclosporine A targets. Bioinformatics. 2014;30:3561–6.
72. Davis TL, Walker JR, Campagna-Slater V, Finerty PJ, Paramanathan R, Bernstein G, et al. Structural and biochemical characterization of the human cyclophilin family of peptidyl-prolyl isomerases. PLoS Biol. 2010;8:e1000439.
73. Akool el S, Gauer S, Osman B, Doller A, Schulz S, Geiger H, et al. Cyclosporin A and tacrolimus induce renal Erk1/2 pathway via ROS-induced and metalloproteinase-dependent EGF-receptor signaling. Biochem Pharmacol. 2012;83:286–95.
74. Rasola A, Sciacovelli M, Chiara F, Pantic B, Brusilow WS, Bernardi P. Activation of mitochondrial ERK protects cancer cells from death through inhibition of the permeability transition. Proc Natl Acad Sci USA. 2010;107:726–31.
75. Frezza C, Cipolat S, Martins de Brito O, Micaroni M, Beznoussenko GV, Rudka T, et al. OPA1 controls apoptotic cristae remodeling independently from mitochondrial fusion. Cell. 2006;126:177–89.
76. Cipolat S, Rudka T, Hartmann D, Costa V, Serneels L, Craessaerts K, et al. Mitochondrial rhomboid PARL regulates cytochrome c release during apoptosis via OPA1-dependent cristae remodeling. Cell. 2006;126:163–75.
77. Lartigue L, Kushnareva Y, Seong Y, Lin H, Faustin B, Newmeyer DD. Caspase-independent mitochondrial cell death results from loss of respiration, not cytotoxic protein release. Mol Biol Cell. 2009;20:4871–84.
78. Tait SW, Oberst A, Quarato G, Milasta S, Haller M, Wang R, et al. Widespread mitochondrial depletion via mitophagy does not compromise necroptosis. Cell Rep. 2013;5:878–85.
79. Waldmeier PC, Feldtrauer JJ, Qian T, Lemasters JJ. Inhibition of the mitochondrial permeability transition by the nonimmunosuppressive cyclosporin derivative NIM811. Mol Pharmacol. 2002;62:22–9.
80. Gao J, Sana R, Calder V, Calonge M, Lee W, Wheeler LA, et al. Mitochondrial permeability transition pore in inflammatory apoptosis of human conjunctival epithelial cells and T cells: effect of cyclosporin A. Investig Ophthalmol Vis Sci. 2013;54:4717–33.
81. Puthalakath H, O'Reilly LA, Gunn P, Lee L, Kelly PN, Huntington ND, et al. ER stress triggers apoptosis by activating BH3-only protein Bim. Cell. 2007;129:1337–49.
82. Misra UK, Gawdi G, Pizzo SV. Cyclosporin A inhibits inositol 1,4,5-trisphosphate binding to its receptors and release of calcium from intracellular stores in peritoneal macrophages. J Immunol. 1998;161:6122–7.
83. Heath-Engel HM, Chang NC, Shore GC. The endoplasmic reticulum in apoptosis and autophagy: role of the BCL-2 protein family. Oncogene. 2008;27:6419–33.
84. Quarato G, Guy CS, Grace CR, Llambi F, Nourse A, Rodriguez DA, et al. Sequential Engagement of Distinct MLKL Phosphatidylinositol-Binding Sites Executes Necroptosis. Mol Cell. 2016;61:589–601.
85. Sentmanat MF, Peters ST, Florian CP, Connelly JP, Pruett-Miller SM. A Survey of Validation Strategies for CRISPR-Cas9 Editing. Sci Rep. 2018;8:888.
86. Connelly JP, Pruett-Miller SM. CRIS.py: A Versatile and High-throughput Analysis Program for CRISPR-based Genome Editing. Sci Rep. 2019;9:4194.
87. Tait SW, Parsons MJ, Llambi F, Bouchier-Hayes L, Connell S, Muñoz-Pinedo C, et al. Resistance to caspase-independent cell death requires persistence of intact mitochondria. Dev Cell. 2010;18:802–13.
88. Otsuki S, Nishimura S, Takabatake H, Nakajima K, Takasu Y, Yagura T, et al. Chemical tagging of a drug target using 5-sulfonyl tetrazole. Bioorg Med Chem Lett. 2013;23:1608–11.

ACKNOWLEDGEMENTS

We thank Dr. Tudor Moldoveanu for providing MEFs *plcγ1*$^{-/-}$ and *plcγ2*$^{-/-}$. Transmission electron microscopy images were acquired at the Cell & Tissue Imaging Center of St. Jude Children's Research Hospital. G.Q. thanks Dr. Tudor Moldoveanu and Prof. Nazzareno Capitanio for a critical review of the manuscript. Cartoons were created with BioRender.com.

AUTHOR CONTRIBUTIONS

GQ, FL, CSG, MA, HS and SN performed the experiments and analyzed the results. SMP-M, JM, JP, ZR and DRG supervised the study and provided access to material and facilities. GQ, FL and DRG conceived and designed the work. GQ and DRG wrote the manuscript. All the authors reviewed the manuscript.

FUNDING

This research was supported by R35CA231620 from the U.S. National Cancer Institute. Transmission electron microscopy images acquisition was supported by St. Jude Children's Research Hospital and NCI P30 CA021765. Center for Advanced Genome Engineering (CAGE) of St. Jude Children's Research Hospital was supported by Cancer Center Grant P30-CA021765. The content is solely the responsibility of the authors and does not necessarily represent the official views of the National Institutes of Health.

COMPETING INTERESTS

The authors declare no competing interests. DRG consults for Inzen Therapeutics and Ventus Therapeutics.

ADDITIONAL INFORMATION

Supplementary information The online version contains supplementary material available at https://doi.org/10.1038/s41418-022-01025-9.

Correspondence and requests for materials should be addressed to Giovanni Quarato or Douglas R. Green.